

1                   **Modal analysis of historical masonry**  
2                   **structures: linear perturbation and software**  
3                   **benchmarking**

4                   Daniele Pellegrini<sup>a</sup>, Maria Girardi<sup>a</sup>, Paulo B. Lourenço<sup>b</sup>, Maria Giovanna  
5                   Masciotta<sup>b</sup>, Nuno Mendes<sup>b</sup>, Cristina Padovani<sup>a</sup>, Luis F. Ramos<sup>b</sup>

6                   <sup>a</sup>*Institute of Information Science and Technologies "A. Faedo", ISTI-CNR, Pisa, Italy*

7                   <sup>b</sup>*ISISE, University of Minho, Department of Civil Engineering, Guimarães, Portugal*

---

8                   **Abstract**

9                   The mechanical behavior of masonry materials has a common feature: a non-  
10                  linear behavior with high compressive strength and very low tensile strength.  
11                  As a consequence, old masonry buildings generally present cracks due to per-  
12                  manent loads and/or accidental events. Therefore, the characterization of  
13                  the global dynamic behavior of masonry structures should take into account  
14                  the presence of existing cracks. This paper presents a numerical approach  
15                  coupling linear perturbation and modal analysis in order to estimate the dy-  
16                  namic properties of masonry constructions, taking into account the existence  
17                  of structural damage. First, the approach is validated on a masonry arch  
18                  subjected to increasing loads, via three FE codes. Then, the same procedure  
19                  is applied to a real masonry structure affected by a severe crack distribution.  
20                  *Keywords:* Masonry-like materials, masonry constructions, modal analysis,  
21                  numerical methods, nonlinear elasticity, linear perturbation

---

## 22 1. Introduction

23 Safeguarding of cultural heritage is an acquired principle nowadays, widely  
24 shared by all communities. Preservation of the past is an indispensable re-  
25 quirement for our society to foster knowledge, awareness of identity, and  
26 ability to think of and plan the future. With regard to architectural her-  
27 itage, age-old buildings and monuments need to be preserved not only from  
28 damage mechanisms and deterioration processes induced by anthropogenic  
29 and environmental actions, but also from the aging effects they are exposed  
30 to during their lifetime. Furthermore, ancient structures are particularly  
31 vulnerable to seismic actions, whose consequences should be prevented - or  
32 at least mitigated - with effective strengthening measures and maintenance  
33 plans. For this purpose, Structural Health Monitoring (SHM) and Finite El-  
34 ement (FE) analysis represent complementary techniques which may help to  
35 understand the complex dynamic behavior of ancient buildings and estimate  
36 the mechanical properties of their constituent materials with use of limited  
37 invasive testing procedures. In addition, if long-term monitoring protocols  
38 are conducted, important information can be caught on the interactions be-  
39 tween the structure under consideration and the surrounding environment  
40 [4], [44], as well as on the evolution of the structural health over time. In  
41 fact, significant changes in the structure's dynamic properties can reveal the  
42 presence of structural damage, as pointed out in [21], [40], [43], where de-  
43 creasing values of natural frequencies were measured at the onset of damage.  
44 Moreover, dynamic monitoring can represent a valuable tool to assess the ef-

45 fectiveness of strengthening interventions, as shown in [33], [34], [44], where  
46 evident rising in the natural frequencies was observed in the monitored his-  
47 torical structures after restoration works.

48 Structural health monitoring is usually coupled with FE analysis via  
49 model updating procedures [1], [2], [5], [10], [12], [46], [52], in order to de-  
50 rive realistic information about the boundary conditions and the mechani-  
51 cal properties of the structure's constituent materials, especially when more  
52 invasive techniques are not viable as in case of heritage buildings. These  
53 procedures typically consist in tuning some parameters of the FE model in  
54 order to minimize the distance between numerical and experimental modal  
55 properties (natural frequencies and mode shapes).

56 In this regard, it is worth noting that modal analysis is carried out within  
57 the framework of linear elasticity. This setting could be unsuited for masonry  
58 buildings, which may exhibit nonlinear behavior even for the self-weight and  
59 sometimes show extended crack patterns. Therefore, the dynamic behavior  
60 of these constructions should be analyzed by taking into account the existing  
61 damage so as to avoid erroneous evaluations of the parameters, which may in  
62 turn compromise the outcome of further numerical simulations. A common  
63 approach to this problem consists in simulating the actual damage observed  
64 on the structure by reducing the stiffness of those finite elements belonging  
65 to the cracked or damaged parts [7], [10], [41], [43].

66 In [23] a numerical procedure implemented in the non commercial FE  
67 software NOSA-ITACA ([www.nosaitaca.it](http://www.nosaitaca.it)) is described. Here, the masonry

68 material is modeled via the masonry-like constitutive equation [14], [30].  
69 This procedure allows evaluating the natural frequencies and mode shapes  
70 of masonry buildings in the presence of cracks, via linear perturbation anal-  
71 ysis and consists of the following steps: first, the initial loads and boundary  
72 conditions are applied to the FE model and the resulting nonlinear equilib-  
73 rium problem is solved through an iterative scheme. Then, a modal analysis  
74 about the equilibrium solution is performed, by using the tangent stiffness  
75 matrix calculated in the last iteration before convergence is reached, thereby  
76 allowing the user to automatically take into account the effects of the stress  
77 distribution on the structure's stiffness.

78 Other applications of linear perturbation, sometimes referred to as pre-  
79 stressed modal analysis, are in the framework of large deformation problems  
80 [13], [24], [36], [53]. With regard to masonry buildings, an example is shown  
81 in [18], where linear perturbation is applied via a commercial code to a his-  
82 toric masonry building.

83 This paper focuses on the use of linear perturbation to evaluate modal  
84 properties of ancient masonry buildings in the presence of cracks. The  
85 method is described in Section 2 and applied to a masonry arch in Section  
86 3, where the results obtained via different constitutive equations and FE  
87 codes (DIANA, MARC, NOSA-ITACA) are compared and discussed. Then,  
88 a real case application is presented in Section 4, where the Mogadouro clock  
89 tower is analyzed via the NOSA-ITACA code, before and after the restora-  
90 tion works carried out in 2005. The paper demonstrates that, by adopting

91 the appropriate constitutive model, different FE codes do provide the same  
92 modal features in the presence of a damaged structure. Moreover, making  
93 use of the experimental results at the authors' disposal [44], [45], it is shown  
94 that linear perturbation analysis combined with finite element modal updat-  
95 ing allows identifying the tower's material properties (i.e. Young's modulus  
96 and tensile strength) that consistently reflect the damaged condition of the  
97 structure before restoration as well as the increase of the structural stiffness  
98 resulting from the subsequent strengthening intervention.

## 99 **2. Constitutive equations, linear perturbation and modal analysis**

100 In recent years the advancement of computer technology and introduc-  
101 tion of innovative mathematical models made it possible to assess the struc-  
102 tural safety of complex ancient masonry buildings by taking into account  
103 the nonlinear behavior of masonry materials, whose response to tension is  
104 completely different from that to compression and whose mechanical char-  
105 acteristics are the result of both their constituent elements and the building  
106 techniques used. The numerous studies conducted in the last decades, aimed  
107 at modeling the behavior of masonry structures, led to the formulation of  
108 different constitutive laws that can be grouped into two main classes. The  
109 first class includes those models in which the macroscopic behavior of the  
110 masonry material is obtained from the micro-mechanical behavior of its sin-  
111 gular components [37], [50], [48], [26], [16], [17]. The second class contains  
112 instead the so-called macro-mechanical models, in which the masonry mate-

113 rial is modeled either as an equivalent continuum [6], [14], [30], [51], [35], or  
114 as an assembly of macro elements with few degrees of freedom characterized  
115 by certain global behaviors [25], [39], [49]. Models originally formulated for  
116 concrete and subsequently applied to masonry structures [9], [47], [11] can be  
117 included in this latter group. A comprehensive review of constitutive models  
118 for masonry falls outside the scope of this paper and the reader is referred  
119 to [27], [28], [29] and [42] for a thorough discussion.

120 When dealing with the analysis of ancient masonry buildings, constitutive  
121 equations belonging to the second class are preferable. In fact, the applica-  
122 tion of micro-mechanical models is not straightforward, since it is difficult  
123 to identify a homogeneous and/or periodic structure in historical masonries.  
124 Moreover, the use of micro-mechanical models requires accurate knowledge  
125 of several parameters related to mechanical properties of the masonry con-  
126 stituent elements, which can not be easily determined; furthermore, the em-  
127 ployment of the micro-mechanical models to complex structures calls for high  
128 computational cost. On the other hand, the application of macro-mechanical  
129 models does require the knowledge of a few parameters, which can be ob-  
130 tained from experimental tests, literature values or even from indications  
131 provided by national building codes and regulations.

132 Among macro-mechanical models, the constitutive equation for low ten-  
133 sion materials, implemented in MARC [32], and the Rankine model, im-  
134 plemented in DIANA [15], are largely adopted to simulate the structural  
135 behavior of masonry constructions. Along with these models, both based

136 on the theory of infinitesimal plasticity, the nonlinear elastic equation of  
 137 masonry-like materials [30] is able to realistically describe the behavior of  
 138 masonry buildings by taking into consideration their zero or low tensile  
 139 strength. This constitutive equation has been implemented in NOSA-ITACA  
 140 [8], [22], a finite element code developed and freely distributed by ISTI-CNR  
 141 ([www.nosaitaca.it](http://www.nosaitaca.it)). Here, masonry is modeled as an isotropic nonlinear elas-  
 142 tic material with zero tensile strength and infinite compressive strength [14].  
 143 It is possible to prove that for every infinitesimal strain tensor  $\mathbf{E}$ , there exists  
 144 a unique triplet  $(\mathbf{T}, \mathbf{E}^e, \mathbf{E}^f)$  of symmetric tensors such that  $\mathbf{E}$  is the sum of  
 145 an elastic strain  $\mathbf{E}^e$  and a positive semidefinite fracture strain  $\mathbf{E}^f$ , and the  
 146 Cauchy stress  $\mathbf{T}$ , negative semidefinite and orthogonal to  $\mathbf{E}^f$ , depends lin-  
 147 early and isotropically on  $\mathbf{E}^e$ , through the Young's modulus  $E$  and Poisson's  
 148 ratio  $\nu$  [14], [30].

149 Masonry-like materials are then characterized by the stress function  $\mathbb{T}$   
 150 given by  $\mathbb{T}(\mathbf{E}) = \mathbf{T}$ , whose explicit expression is reported in [30], along with  
 151 its properties. In particular,  $\mathbb{T}$  is differentiable in an open dense subset of  
 152 the set of all strains [38] and the derivative  $D_E \mathbb{T}(\mathbf{E})$  of  $\mathbb{T}(\mathbf{E})$  with respect  
 153 to  $\mathbf{E}$  is a positive semidefinite symmetric fourth-order tensor, whose explicit  
 154 expression is reported in [30]. The equation of masonry-like materials has  
 155 been then generalized in order to take into account a weak tensile strength  
 156  $\sigma_t \geq 0$  [30].

157 The constitutive law of low tensile materials implemented in MARC [32]  
 158 is based on the nonlinear concrete cracking formulation described in [9]. Ma-

159 sonry is modeled as a nonlinear isotropic material in which a crack can de-  
160 velop orthogonal to the direction of the maximum principal stress, when it  
161 exceeds the strength of the material  $\sigma_t$ . After the occurrence of the first  
162 crack, a second crack may arise orthogonal to the first. In the same way, a  
163 third crack could open perpendicularly to the first two. In this situation the  
164 material loses all its load-carrying capacity across the crack, except when a  
165 tension softening behavior is considered, which can have a linear trend with  
166 slope equal to  $E_s$ .

167 The Rankine plasticity model implemented in DIANA [15] employs the  
168 Rankine yield criterion to simulate tensile cracking in concrete and rock  
169 under monotonic loading conditions. The yield function depends on both the  
170 maximum principal stress and a yield value  $\tilde{\sigma}_t$  that describes the nonlinear  
171 exponential tensile softening behavior of the material, involving the tensile  
172 strength  $\sigma_t$  and the fracture energy  $G_f^I$  [19].

173 Although the mechanical behavior of masonry constructions is clearly  
174 nonlinear, modal analysis, which is based on the assumption that masonry  
175 constituent materials feature a linear elastic behavior, is widely used in prac-  
176 tical applications. Indeed, it provides important qualitative information on  
177 the global dynamic behavior of masonry structures, thereby allowing to as-  
178 sess their seismic vulnerability in compliance with the Italian and European  
179 regulations. On the other hand, traditional modal analysis does not take into  
180 account the influence that both the nonlinear behavior of the masonry mate-  
181 rial and the presence of cracked regions can have on the natural frequencies

182 of masonry structures. While the effects of cracks on the vibration frequen-  
183 cies are taken into account in different fields of mechanical and aerospace  
184 engineering through the so-called linear perturbation analysis, such effects  
185 are not fully explored yet as far as the civil engineering field is concerned.

186 In this paper the linear perturbation approach is coupled with modal  
187 analysis, with the aim of assessing the dependence of the dynamic properties  
188 of a masonry structure on the stress field and crack distribution induced by  
189 the loads acting on the structure. Apart from the examples described in [23],  
190 where a masonry beam, an arch on piers and the San Frediano bell tower in  
191 Lucca have been analyzed, coupling linear perturbation and modal analysis is  
192 far from being fully investigated, although it allows for calculating the natural  
193 frequencies and mode shapes of a masonry body exhibiting a crack distribu-  
194 tion due to the applied loads. In this regard, the procedure implemented in  
195 the NOSA-ITACA code consists in calculating the numerical solution to the  
196 nonlinear equilibrium problem of a masonry structure discretized into finite  
197 elements, subjected to given boundary and loading conditions, and then con-  
198 sidering the linear equation governing the undamped free vibrations of the  
199 structure about the equilibrium state

$$M\ddot{u} + K_T u = 0. \quad (1)$$

200 In equation (1)  $u$  is the displacement vector, which belongs to  $\mathbb{R}^n$  and  
201 depends on time  $t$ ,  $\ddot{u}$  is the second-derivative of  $u$  with respect to  $t$ , and

202  $K_T$  and  $M \in \mathbb{R}^{n \times n}$  are the tangent stiffness and mass matrices of the finite-  
 203 element assemblage. Note that  $K_T$  is symmetric and positive semidefinite,  
 204  $M$  is symmetric and positive definite. Equation (1) is similar to the equation  
 205 of the motion of a linear elastic body, though here the elastic stiffness matrix,  
 206 calculated using the elasticity tensor, is replaced by the tangent stiffness ma-  
 207 trix  $K_T$ , calculated using the solution to the equilibrium problem and then  
 208 takes into account the presence of cracks in body.

209

210 By assuming that

$$u = \phi \sin(\omega t), \quad (2)$$

211 with  $\phi$  a vector of  $\mathbb{R}^n$  and  $\omega$  a real scalar, equation (1) can be transformed  
 212 into the constrained generalized eigenvalue problem

$$K_T \phi = \omega^2 M \phi, \quad (3)$$

213

$$T \phi = 0, \quad (4)$$

214 with  $T \in \mathbb{R}^{m \times n}$  and  $m \ll n$ .

215

216 Condition (4) expresses the fixed constraints and the master-slave rela-  
 217 tions assigned to displacement  $u$ , written in terms of vector  $\phi$ . The restriction  
 218 of the matrix  $K_T$  to the null subspace of  $\mathbb{R}^n$  defined by (4) is positive definite.

219 Therefore, given the structure under examination, discretized into finite  
220 elements, and given the mechanical properties of the constituent materials  
221 together with the kinematic constraints and loads acting on the structure,  
222 the procedure implemented in NOSA-ITACA consists of the following steps.

223 Step 1. A preliminary modal analysis is conducted by assuming the struc-  
224 ture's constituent material to be linear elastic, with stiffness matrix  $K$ . The  
225 generalized eigenvalue problem (3)-(4) is then solved, with  $K$  in place of  $K_T$ ,  
226 and the natural frequencies  $f_{i,E} = \omega_{i,E}/2\pi$  and mode shapes  $\phi_i^E$  calculated.

227 Step 2. The solution of the nonlinear equilibrium problem of the structure  
228 is found and the derivative of the stress function needed to calculate the  
229 tangent stiffness matrix  $K_T$  to be used in the next step is evaluated.

230 Step 3. The generalized eigenvalue problem (3)-(4) is finally solved and  
231 the natural frequencies  $f_i = \omega_i/2\pi$  of the structure in the presence of cracks  
232 are estimated.

233 Similar procedures based on linear perturbation followed by modal analy-  
234 sis are implemented in MARC and DIANA. The three codes NOSA-ITACA,  
235 MARC and DIANA, which adopt different constitutive equations for ma-  
236 sonry, have been used with the twofold aim of (1) studying the static behavior  
237 of a masonry arch subjected to its own weight and a vertical concentrated  
238 load and, after a linear perturbation, (2) assessing the dependence of the  
239 natural frequencies and mode shapes on the crack distribution. The results  
240 of this comparative study are reported in Section 3 and show that, in spite of

241 the different constitutive equations adopted, the dependence of the dynami-  
242 cal properties of the arch on the loads is very similar for the three codes.

### 243 **3. Application to a masonry arch and software benchmarking**

244 The numerical method for modal analysis described in Section 2 is here  
245 applied to the semi-circular masonry arch shown in Figure 1. The system is  
246 fully clamped at the springings and its geometry features a mean radius of  
247 0.77 m, a span of 1.50 m, a cross section of 0.16 m  $\times$  1 m and a springing angle  
248 of about 13°. The arch is subjected to a plane stress state due to its self-  
249 weight and to a concentrated load P applied at the extrados at a quarter of  
250 the span. The arch is discretized into 784 8-node isoparametric quadrilateral  
251 elements with quadratic shape functions (corresponding to element 2, 26  
252 and CQ16M of the NOSA-ITACA [8], MARC [32] and DIANA [15] libraries,  
253 respectively), for a total of 2565 nodes. Figure 2 shows the mesh generated  
254 by NOSA-ITACA, later converted in the MARC and DIANA format.

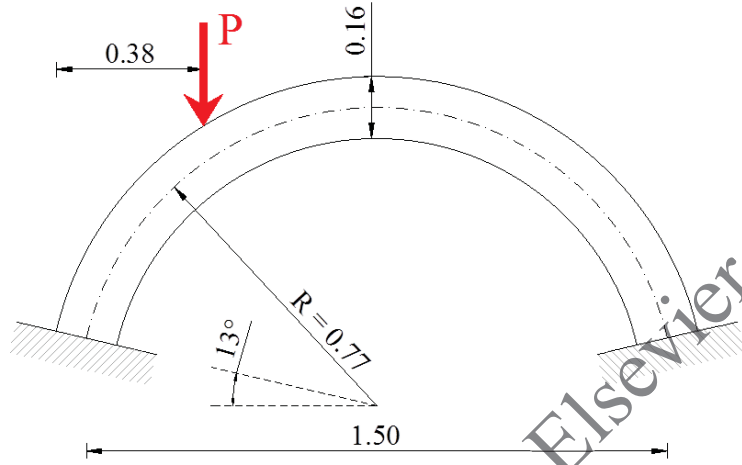


Figure 1: Geometry of the arch (length in meters).

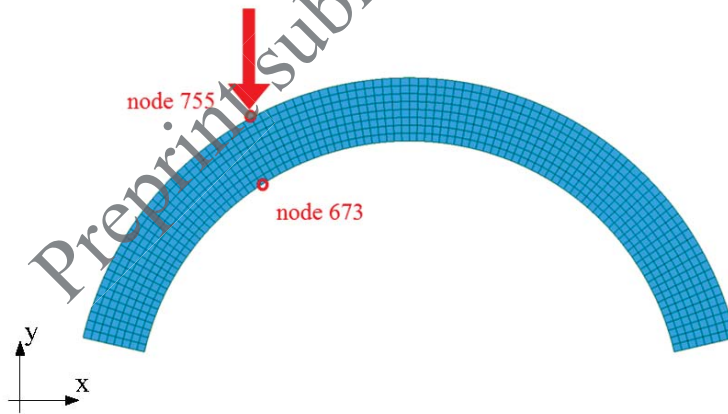


Figure 2: Mesh of the arch created by NOSA-ITACA code.

255 The numerical analyses conducted with NOSA-ITACA, MARC and DI-  
 256 ANA have manifold goals. Firstly, they are aimed at analysing the static

257 behavior of the arch modeled by adopting three different constitutive equa-  
258 tions. Secondly they allow comparing the natural frequencies of the arch in  
259 the linear elastic case with those in the presence of the damage induced by  
260 the increasing vertical load. Several parametric numerical experiments have  
261 been carried out, as the tensile strength  $\sigma_t$  of the material varies, revealing  
262 that, in the presence of cracks, the values of the frequencies calculated by  
263 the three codes are comparable.

264 A preliminary modal analysis (step 1, Section 2) was performed by as-  
265 suming the arch made of a linear elastic material with Young's modulus  
266  $E = 3 \cdot 10^9$  Pa, Poisson's ratio  $\nu = 0.2$  and mass density  $\rho = 1930$  kg/m<sup>3</sup>.  
267 The first four corresponding natural frequencies  $f_{i,E}$  ( $i = 1..4$ ) (calculated  
268 by the three codes) are

269

$$270 \quad f_{1,E} = 92.33 \text{ Hz}; f_{2,E} = 163.64 \text{ Hz}; f_{3,E} = 266.95 \text{ Hz}; f_{4,E} = 297.95 \text{ Hz}.$$

271 Then, by following the procedure outlined in Section 2, step 2, damage  
272 was induced in the arch by applying the self-weight along with an incremen-  
273 tal vertical load. At each increment the frequencies  $f_{i,j}$  (the  $i$ -th frequency  
274 calculated by  $j$ -th code: N (NOSA-ITACA), M (MARC) and D(DIANA))  
275 and the corresponding mode shapes were calculated.

276 In order to perform nonlinear static analysis in DIANA and MARC, the  
277 parameters  $G_f^I$  and  $E_s$  (see Section 2) have to be assigned, in addition to the  
278 tensile strength  $\sigma_t$ , set to vary from 0 Pa to  $5 \cdot 10^4$  Pa. The Mode-I fracture

279 energy with  $G_f^I = 25 \text{ Nm/m}^2$  was assumed in DIANA, while  $E_s$  was calcu-  
280 lated, for each analysis performed in MARC, by imposing the equivalence  
281 between the areas below the softening curves of both codes.

282 The value of the vertical load applied to the arch was increased through eight  
283 increments from 0 kN to 4 kN. Each analysis was repeated by decreasing the  
284 value of  $\sigma_t$  from  $5 \cdot 10^4 \text{ Pa}$  to  $5 \cdot 10^3 \text{ Pa}$ . For values of  $\sigma_t$  lower than  $5 \cdot 10^3 \text{ Pa}$ ,  
285 only NOSA-ITACA and DIANA reach the convergence for any value of the  
286 vertical load.

287 It is pointed out that in terms of displacement, stress and cracking fields,  
288 the results provided by the three codes show very good agreement for each  
289 value of the vertical load up to a tensile stress of  $5 \cdot 10^3 \text{ Pa}$ . Figures 3, 4,  
290 5, 6 and 7 display for the three codes the plots relevant to the norm of dis-  
291 placements, the components of the Cauchy stress tensor and the maximum  
292 eigenvalue of the fracture strain, calculated for  $\sigma_t = 5 \cdot 10^3 \text{ Pa}$  and  $P = 4 \text{ kN}$ .  
293 Despite the different constitutive equations adopted, NOSA-ITACA and DI-  
294 ANA provide the same results, whereas the values obtained in MARC exhibit  
295 an increment of about 5 – 10% with respect to the afore-mentioned codes.

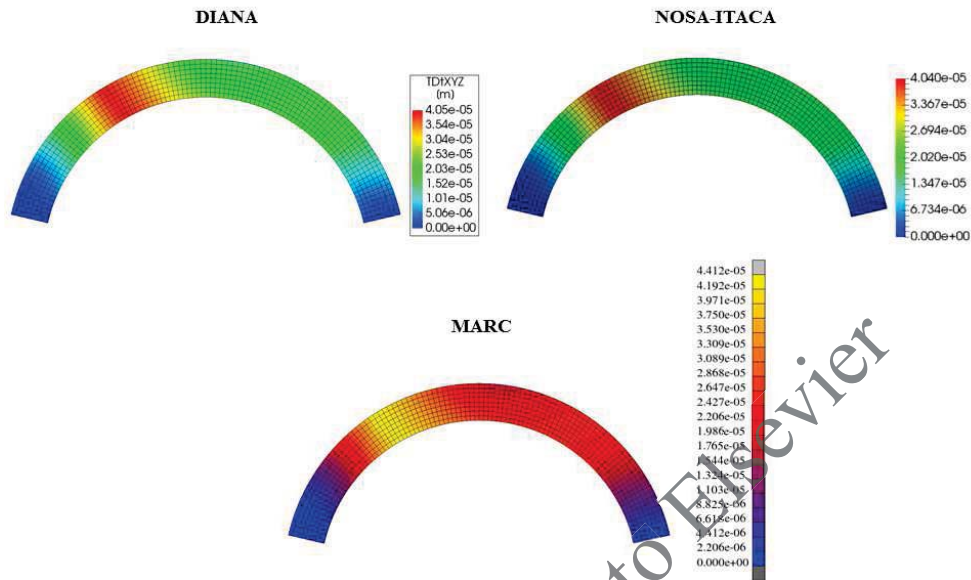


Figure 3: Norm of displacement [m] ( $P = 4 \text{ kN}$ ,  $\sigma_t = 5 \cdot 10^3 \text{ Pa}$ ).

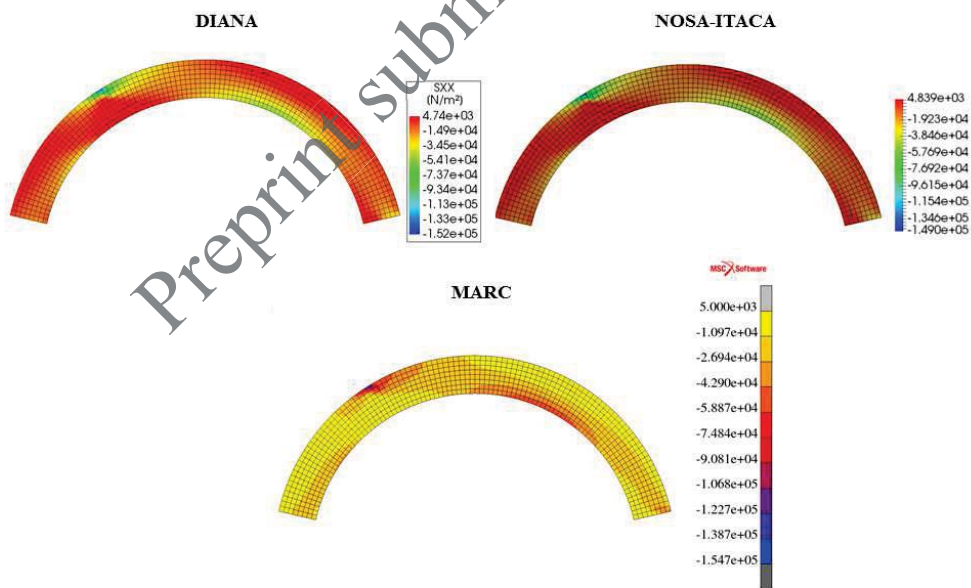


Figure 4: Cauchy stress component  $\sigma_x$  [Pa] ( $P = 4 \text{ kN}$ ,  $\sigma_t = 5 \cdot 10^3 \text{ Pa}$ ).

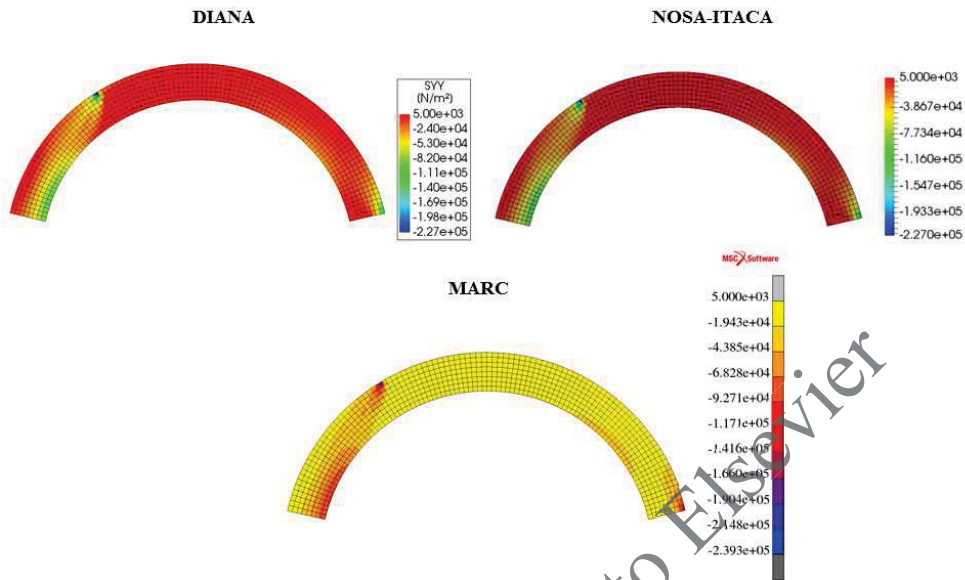


Figure 5: Cauchy stress component  $\sigma_y$  [Pa] ( $P = 4$  kN,  $\sigma_t = 5 \cdot 10^3$  Pa).

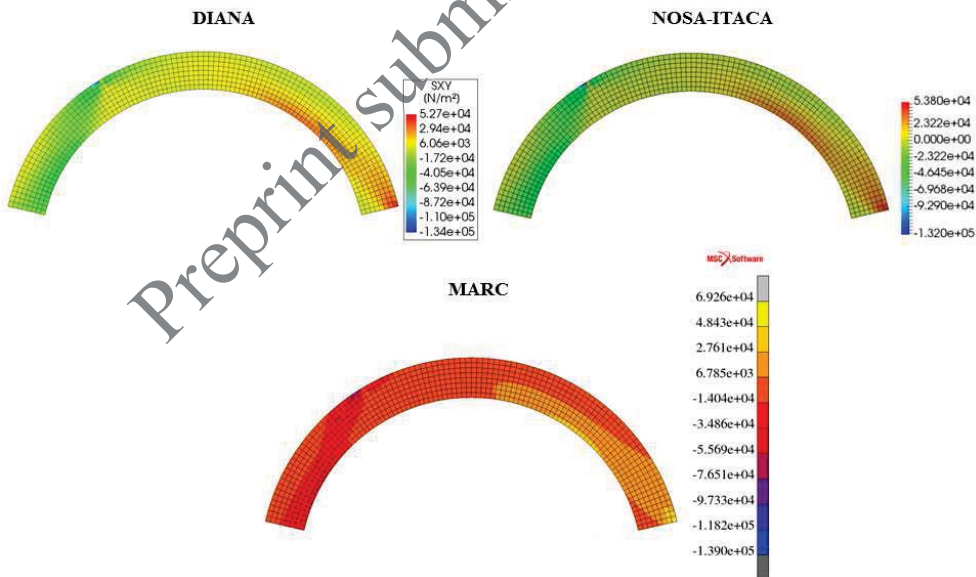


Figure 6: Cauchy stress component  $\tau_{xy}$  [Pa] ( $P = 4$  kN,  $\sigma_t = 5 \cdot 10^3$  Pa).

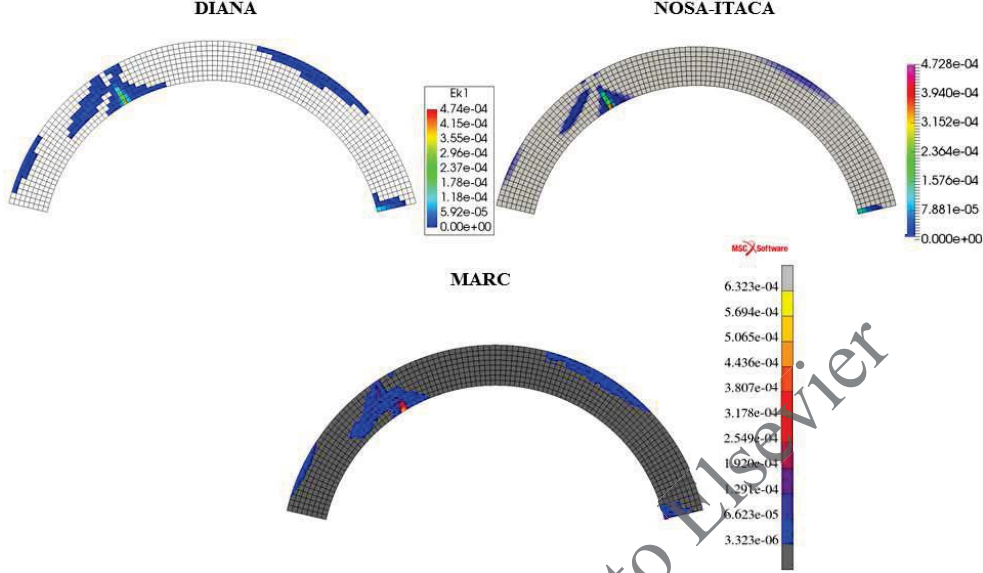


Figure 7: Maximum eigenvalue of the fracture strain tensor ( $P = 4 \text{ kN}$ ,  $\sigma_t = 5 \cdot 10^3 \text{ Pa}$ ).

296 Figures 8, 9, 10, 11 show the variation of the first four frequencies  $f_{i,j}$   
 297 of the arch, calculated in the three codes via linear perturbation analysis,  
 298 versus decreasing values of tensile strength  $\sigma_t$  for  $P = 3 \text{ kN}$  (continuous line)  
 299 and  $P = 4 \text{ kN}$  (dashed line). The corresponding mode shapes for the linear  
 300 elastic case are also shown. Tables 1, 2, and 3, 4 report, for the same load  
 301 conditions  $P$ , the values of  $\sigma_t$  used in the different analyses along with the  
 302 corresponding relative frequency errors  $\delta_{i,j}$  defined by

$$\delta_{i,j} = \frac{(f_{i,E} - f_{i,j})}{f_{i,E}}, \quad \text{for } i = 1 \dots 4 \quad \text{and } j = N, M, D \quad (5)$$

303 where  $f_{i,E}$  is the  $i$ -th frequency calculated by standard modal analysis and  
 304  $f_{i,j}$  the  $i$ -th frequency calculated by  $j$ -th code via linear perturbation analysis,

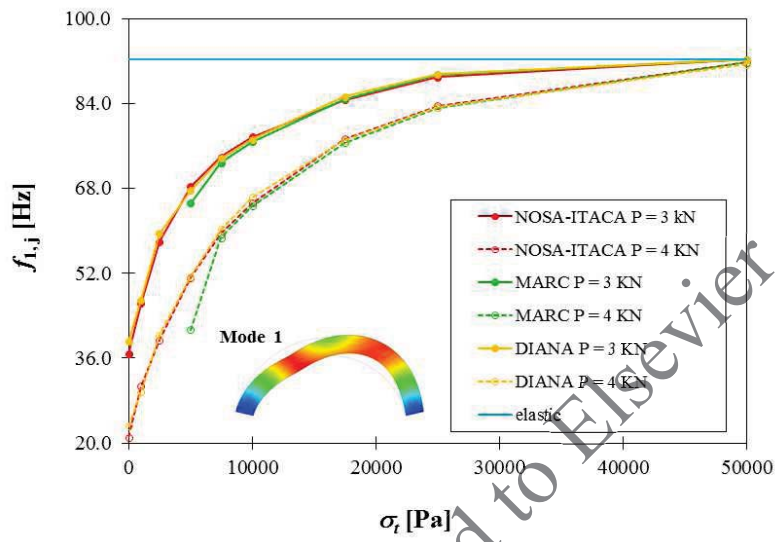


Figure 8: First frequency  $f_{1,j}$  versus tensile strength  $\sigma_t$  for  $P = 3$  kN (continuous line) and  $P = 4$  kN (dashed line).

Preprint submitted to Elsevier

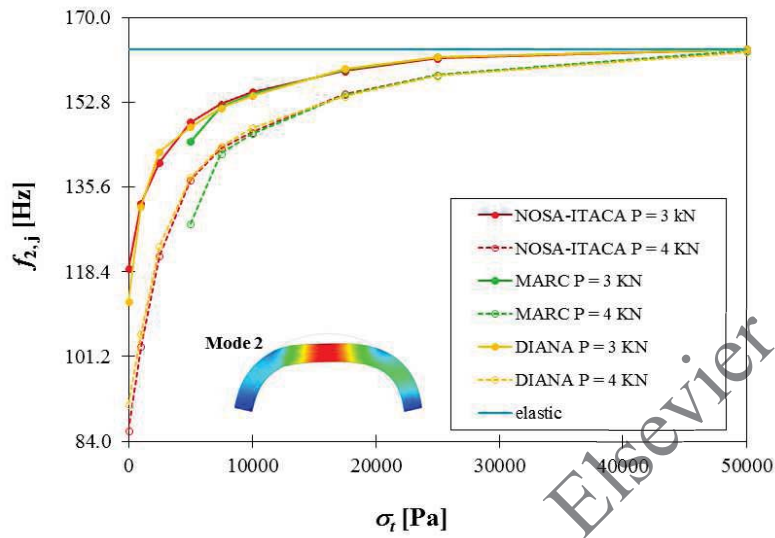


Figure 9: Second frequency  $f_{2,j}$  versus tensile strength  $\sigma_t$  for P = 3 kN (continuous line) and P = 4 kN (dashed line).

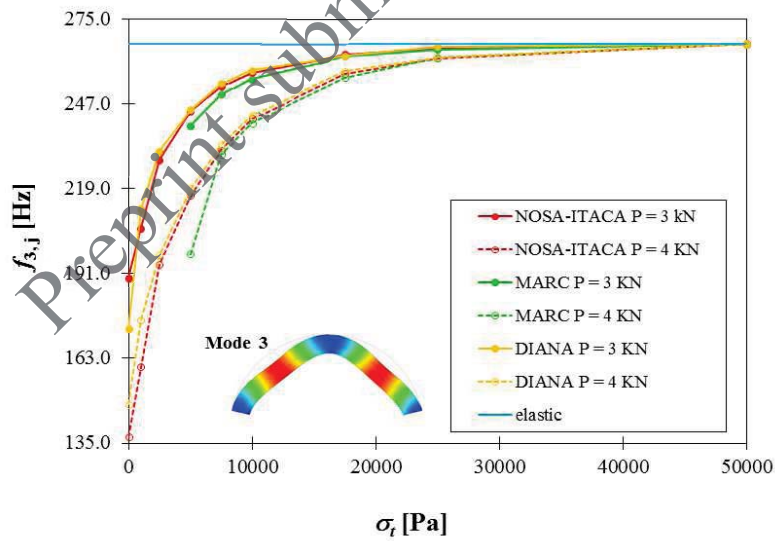


Figure 10: Third frequency  $f_{3,j}$  versus tensile strength  $\sigma_t$  for P = 3 kN (continuous line) and P = 4 kN (dashed line).

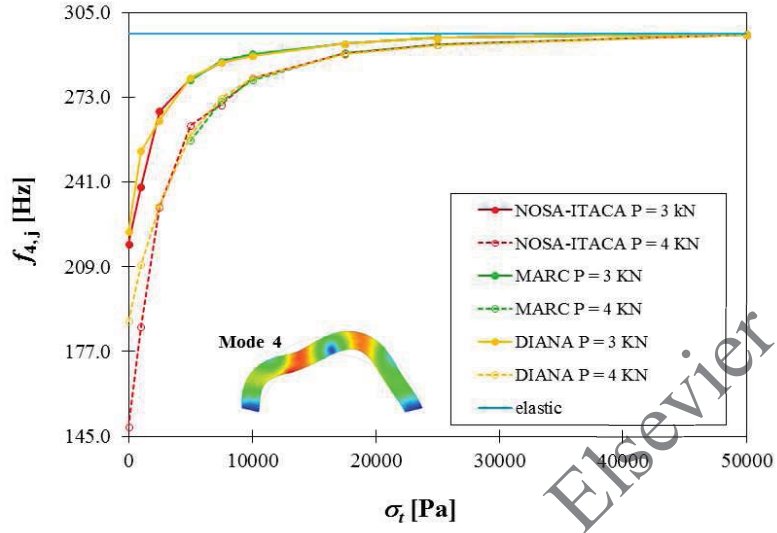


Figure 11: Fourth  $f_{4,j}$  versus tensile strength  $\sigma_t$  for  $P = 3$  kN (continuous line) and  $P = 4$  kN (dashed line).

$\sigma_t$ [Pa]	$\delta_{1,N}$ [%]	$\delta_{1,M}$ [%]	$\delta_{1,D}$ [%]	$\delta_{2,N}$ [%]	$\delta_{2,M}$ [%]	$\delta_{2,D}$ [%]
0	60.20	-	57.61	27.28	-	31.28
1000	49.80	-	49.13	19.09	-	19.47
2500	37.21	-	35.52	14.03	-	12.74
5000	25.93	29.35	26.68	9.06	11.45	9.63
7500	19.81	21.07	20.19	6.79	7.15	7.26
10000	15.80	16.77	16.26	5.32	5.60	5.75
17500	8.20	8.06	7.57	2.67	2.51	2.38
25000	3.56	3.06	2.89	1.14	0.95	0.95
50000	0.00	0.00	0.00	0.00	0.00	0.00

Table 1:  $\delta_{i,j}$ ,  $i = 1,2$  ;  $j = N, M, D$  ;  $P = 3$  kN.

$\sigma_t$ [Pa]	$\delta_{3,N}$ [%]	$\delta_{3,M}$ [%]	$\delta_{3,D}$ [%]	$\delta_{4,N}$ [%]	$\delta_{4,M}$ [%]	$\delta_{4,D}$ [%]
0	28.95	–	35.24	26.71	–	25.08
1000	22.86	–	20.45	19.43	–	14.92
2500	14.42	–	13.31	9.81	–	10.99
5000	8.36	10.21	8.17	5.66	5.88	5.56
7500	5.29	6.24	4.92	3.63	3.47	3.65
10000	3.52	4.30	3.19	2.69	2.54	2.77
17500	1.35	1.57	1.47	1.21	1.19	1.21
25000	0.60	0.70	0.39	0.50	0.41	0.45
50000	0.00	0.00	0.00	0.00	0.00	0.00

Table 2:  $\delta_{i,j}$ ,  $i = 3,4$  ;  $j = N, M, D$  ;  $P = 3$  kN.

$\sigma_t$ [Pa]	$\delta_{1,N}$ [%]	$\delta_{1,M}$ [%]	$\delta_{1,D}$ [%]	$\delta_{2,N}$ [%]	$\delta_{2,M}$ [%]	$\delta_{2,D}$ [%]
0	77.20	–	74.92	47.38	–	44.10
1000	66.79	–	67.90	36.94	–	35.28
2500	57.29	–	56.32	25.63	–	24.42
5000	44.50	55.15	44.38	16.19	21.67	15.91
7500	35.57	36.42	34.72	12.32	12.95	12.03
10000	29.27	29.94	28.12	10.32	10.50	9.76
17500	16.15	17.01	16.45	5.53	5.62	5.81
25000	9.42	9.80	9.66	3.19	3.20	3.28
50000	0.56	0.51	0.95	0.19	0.17	0.34

Table 3:  $\delta_{i,j}$ ,  $i = 1,2$  ;  $j = N, M, D$  ;  $P = 4$  kN.

$\sigma_t$ [Pa]	$\delta_{3,N}$ [%]	$\delta_{3,M}$ [%]	$\delta_{3,D}$ [%]	$\delta_{4,N}$ [%]	$\delta_{4,M}$ [%]	$\delta_{4,D}$ [%]
0	48.70	–	44.65	50.06	–	36.55
1000	40.01	–	34.17	37.21	–	29.39
2500	27.26	–	26.15	22.03	–	21.90
5000	18.79	26.05	17.98	11.59	13.52	12.88
7500	13.17	13.71	12.54	9.02	8.58	8.16
10000	9.26	9.82	8.84	5.62	5.83	5.60
17500	3.72	4.24	3.45	2.46	2.40	2.55
25000	1.79	1.76	1.70	1.35	1.34	1.43
50000	0.08	0.08	0.04	0.08	0.07	0.13

Table 4:  $\delta_{i,j}$ ,  $i = 3,4$  ;  $j = N, M, D$  ;  $P = 4$  kN.

306 As expected, the figures highlight that the frequencies of the arch decrease  
307 as the vertical load increases and the tensile strength decreases. As outlined  
308 in Tables 1, 2, 3 and 4, regardless of the value of the vertical load, the  
309 fundamental frequency falls faster than the other frequencies; approximately  
310 27% against 9%, when  $P = 3$  kN and  $\sigma_t = 5 \cdot 10^3$  Pa, and 50% against 20%,  
311 when  $P = 4$  kN and  $\sigma_t = 5 \cdot 10^3$  Pa. This is due to the chosen vertical load  
312 position, which induces a deformation in the arch similar to the first mode  
313 shape (Figure 12, 13).  
314 Figure 12 shows the mode shapes corresponding to the first four frequencies  
315 of the arch for  $\sigma_t = 5 \cdot 10^3$  Pa and  $P = 3$  kN. Figure 13 shows the same  
316 four mode shapes but for  $\sigma_t = 5 \cdot 10^3$  Pa and  $P = 4$  kN. The figures report  
317 the degree of consistency, expressed in terms of MAC, viz. Modal Assurance  
318 Criterion [31], calculated between the  $i$ -th mode shape of the damaged arch  
319 and the corresponding mode shape calculated via standard modal analysis.  
320 It is noticed that frequencies are much more sensitive than mode shapes to

321 damage; for example when  $\sigma_t = 5 \cdot 10^3$  Pa and  $P = 3$  kN, the first frequency  
 322 shows a relative variation of about 25% while the MAC value is equal to  
 323 0.99, whereas when  $\sigma_t = 5 \cdot 10^3$  Pa and  $P = 4$  kN, the first frequency has  
 324 a relative downshift of about 50% (which indeed corresponds to a severe  
 325 damage condition), but the MAC still continues to be rather high, showing  
 326 values not lower than 0.90.

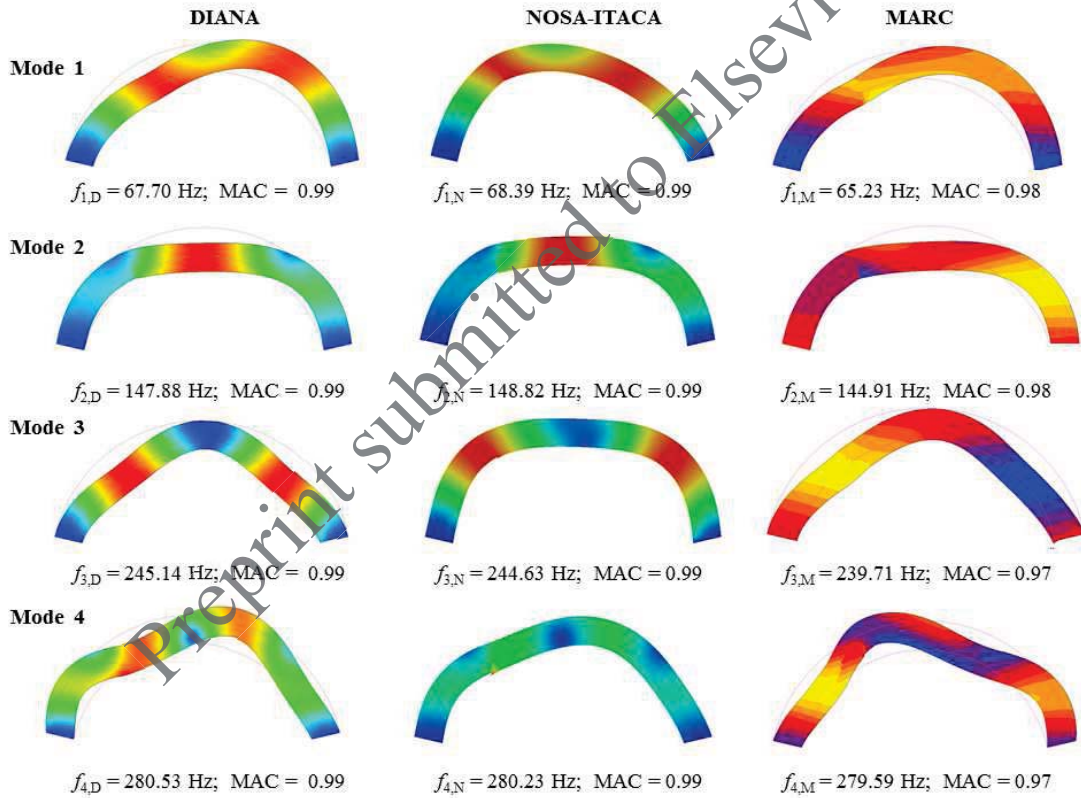


Figure 12: First four mode shapes of the damaged arch ( $P = 3$  kN,  $\sigma_t = 5 \cdot 10^3$  Pa).

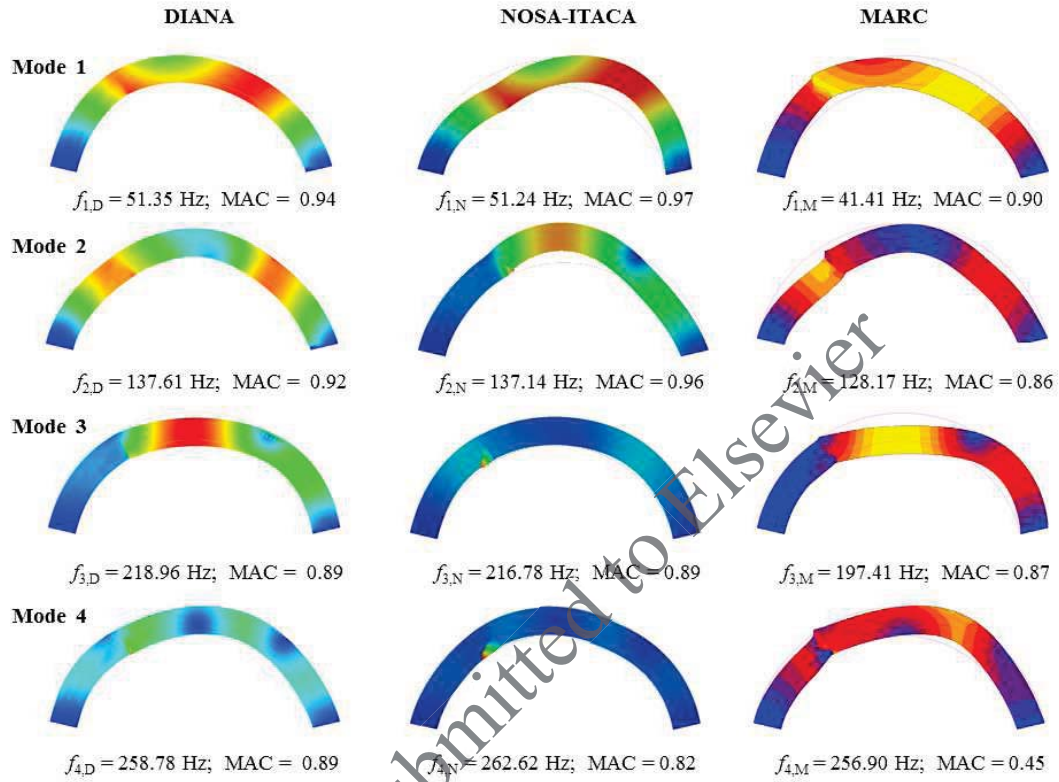


Figure 13: First four mode shapes of the damaged arch ( $P = 4$  kN,  $\sigma_t = 5 \cdot 10^3$  Pa).

327 In order to validate the frequencies values calculated by the three FE  
 328 codes, the load-displacement curves corresponding to  $\sigma_t = 5 \cdot 10^3$  Pa were  
 329 plotted (Figure 14) for nodes 755 and 673, positioned respectively at the  
 330 application point of vertical load and the corresponding point at the intrados  
 331 of the arch (Figure 2).

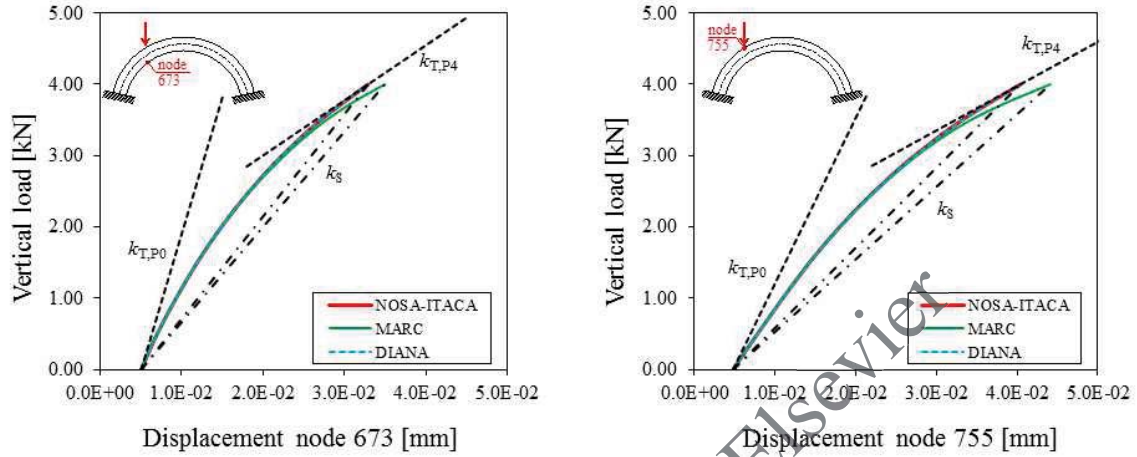


Figure 14: Vertical load versus displacement magnitude of node 673 (on the left) and node 755 (on the right),  $\sigma_t = 5 \cdot 10^3$  Pa.

332 For each curve, its fourth-degree interpolating polynomial is determined  
 333 and then the slopes  $k_{T,P0}$  and  $k_{T,P4}$  of the tangents at the origin and at P =  
 334 4 kN, (dashed lines in Figure 14) are calculated. The slope  $k_S$  of the secant  
 335 passing for those points (dashed-dot lines in Figure 14) is also calculated.  
 336 Since the loss of frequency is expected to be related to the square root of the  
 337 loss of stiffness (mass being equal), the following quantities were calculated as  
 338 for the first frequency, i.e. the one suffering a major decrease due to damage

$$\tilde{f}_{1,T} = f_{1,E} \cdot \sqrt{\frac{k_{T,P4}}{k_{T,P0}}}, \quad (6)$$

$$\tilde{f}_{1,S} = f_{1,E} \cdot \sqrt{\frac{k_S}{k_{T,P0}}}, \quad (7)$$

339 The results obtained are summarized in Tables 5 and 6 for all the three  
340 codes. It is worth noting that the first frequency  $\tilde{f}_{1,T}$  calculated by using the  
341 tangent stiffness is a good approximation of the frequency  $f_{1,j}$  computed via  
342 linear perturbation analysis, whereas the choice of the secant stiffness matrix  
343 would lead to an overestimation of the frequency of the damaged structure.

Code	P [kN]	$k_T$ [kN/m]	$k_S$ [kN/m]	$\tilde{f}_{1,T}$ [Hz]	$\tilde{f}_{1,S}$ [Hz]	$f_{1,j}$ [Hz]
N	0	254.48	143.52	50.87	69.34	51.24
	4	77.26				
M	0	260.23	133.68	41.76	66.18	41.41
	4	53.23				
D	0	254.48	143.55	50.88	69.34	51.35
	4	77.28				

Table 5: Comparison of the first frequency of the arch using the tangent stiffness  $k_T$  and the secant stiffness  $k_S$  evaluated in node 673 with the numerical frequency obtained via linear perturbation analysis.

Code	P [kN]	$k_T$ [kN/m]	$k_S$ [kN/m]	$\tilde{f}_{1,T}$ [Hz]	$\tilde{f}_{1,S}$ [Hz]	$f_{1,j}$ [Hz]
N	0	180.68	112.31	54.16	72.79	51.24
	4	62.16				
M	0	173.20	133.68	46.54	70.75	41.41
	4	53.23				
D	0	180.68	114.69	54.78	73.56	51.35
	4	63.61				

Table 6: Comparison of the first frequency of the arch using the tangent stiffness  $k_T$  and the secant stiffness  $k_S$  evaluated in node 755 with the numerical frequency obtained via linear perturbation analysis.

#### 344 4. Application to a real case study: the Mogadouro clock tower

##### 345 4.1. Description of the case study

346 The Mogadouro clock tower (Figure 15) is a historic masonry structure  
347 located inside the castle perimeter of the homonymous town in the Northeast  
348 of Portugal and likely built after 1559 to serve the neighbouring church as  
349 a bell tower. The fabric features a rectangular cross section of  $4.7 \times 4.7 \text{ m}^2$ ,  
350 with masonry walls of about 1 m thickness, and a height of 20.4 m. The  
351 central part of the walls is built of rubble stones with thick mortar joints,  
352 whereas the corners are made of large granite units with dry joints. Eight  
353 masonry columns support the roof body, forming two rectangular openings  
354 of about  $0.9 \times 2.0 \text{ m}^2$  per façade.

Preprint submitted to Elsevier



Figure 15: Clock tower and castle of Mogadouro.

355 Due to the lack of maintenance, the tower did appear in very poor condi-  
356 tions. Beyond material degradation and biological growth, out-of-plane dis-  
357 placements and cracks could be clearly observed. The most damaged parts  
358 were the East and West façades, where two deep passing cracks were about  
359 to separate the box cross section of the tower into two U halves (Figures 16,  
360 17). As the structural safety was jeopardized, rehabilitation works aimed at  
361 reinstating the sound condition of the structure were carried out in 2005.  
362 The intervention included: lime grout injections for sealing and walls consol-  
363 idation, substitution of deteriorated material, and installation of pre-stressed  
364 tie-rods to restrain cracks from possible reopening.

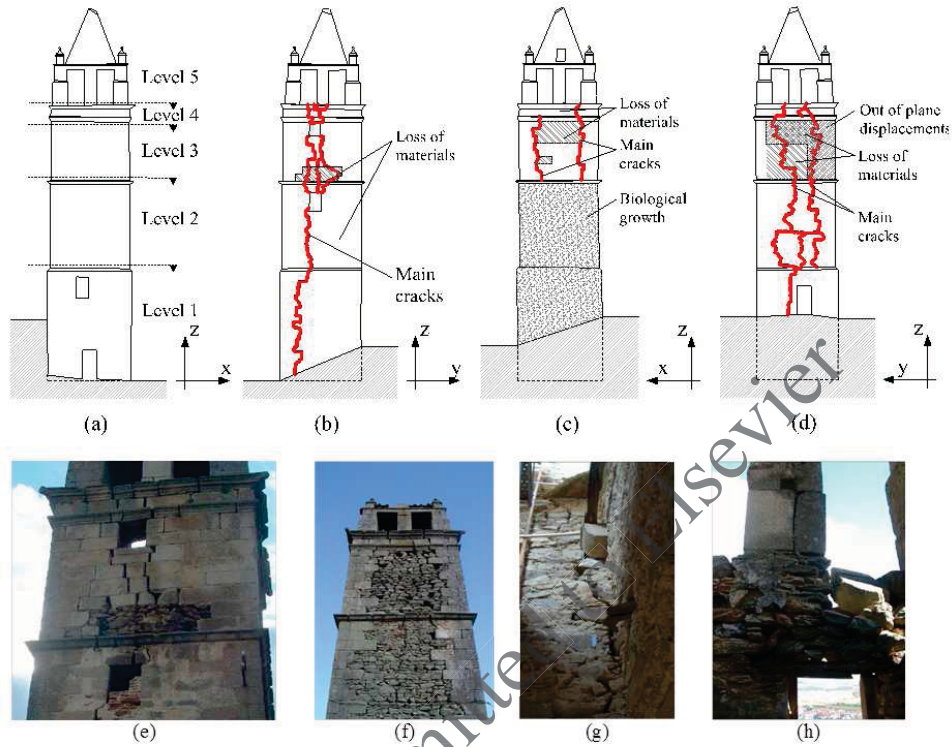


Figure 16: Damage in the tower: (a) South, (b) East, (c) North and (d) West façades; cracks on the (e) East and (f) West fronts; (g) inner crack in the West façade; and (h) example of material loss [44], [45].

#### 365 4.2. Dynamic identification of the tower before and after rehabilitation

366 To evaluate the structural response pre- and post-rehabilitation, two cam-  
 367 paigns of Ambient Vibrations Tests (AVTs) were carried out making use of  
 368 ambient excitation sources, such as wind and traffic [44], [45]. The response  
 369 of the tower was measured in 54 selected points distributed along three lev-  
 370 els, according to the layout displayed in Figure 17. The dynamic equipment  
 371 consisted of 4 uniaxial piezoelectric accelerometers with a bandwidth rang-  
 372 ing from 0.15 to 1000 Hz (5%), a dynamic range of  $\pm 0.5g$ , a sensitivity of

373 10 V/g,  $8\mu\text{g}$  of resolution and 0.21 kg of weight, connected by coaxial cables  
374 to a front-end data acquisition system with a 24-bit ADC, provided with  
375 anti-aliasing filters. The front-end was connected to a laptop by an Ethernet  
376 cable. The accelerometers were bolted to aluminium plates, which were in  
377 turn glued to the stones through an epoxy layer. As the acquisition system  
378 was composed only by 4 channels, 27 test setups were necessary to record  
379 the accelerations in all selected measurement points. A preliminary FE dy-  
380 namic analysis assisted in the selection of the acquisition parameters. Thus,  
381 to ensure an acquisition time window 2000 times larger than the estimated  
382 fundamental period of the structure, the output signals were recorded with  
383 a sampling frequency of 256 Hz for a duration of about 11 minutes. Same  
384 test planning and measurement points were adopted before and after the  
385 reinstatement works.

Preprint submitted to Elsevier

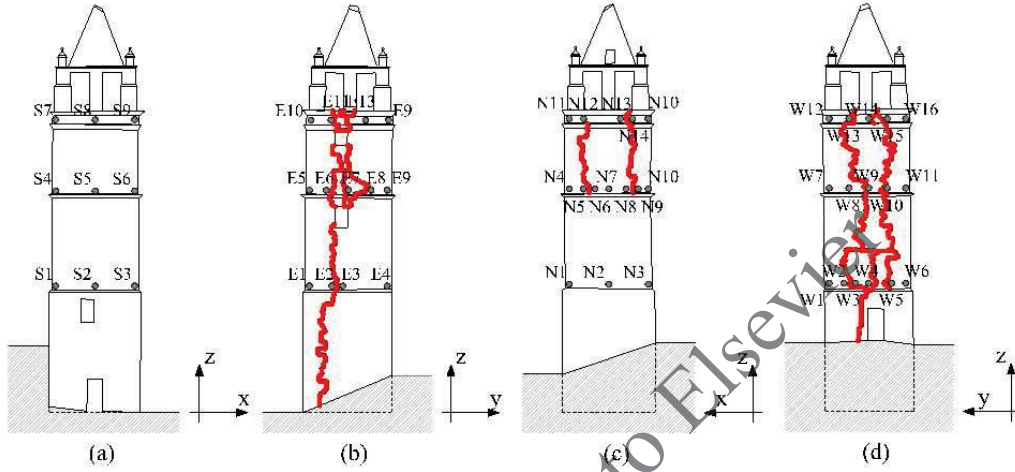


Figure 17: Sensor layout for AVTs: (a) South, (b) East, (c) North and (d) West façades [44], [45].

386 For each structural condition (before and after rehabilitation), the modal  
 387 parameters were estimated by comparing the results from two established and  
 388 complementary OMA techniques: the Enhanced Frequency Domain Decom-  
 389 position (EFDD) method and the Stochastic Subspace Identification (SSI)  
 390 method, both implemented in ARTeMIS software [3]. In total, seven modes  
 391 of vibration were identified in the frequency ranges 2-9 Hz and 2-17 Hz for  
 392 the damaged and undamaged conditions, respectively. Tables 7 and 8 sum-  
 393 marize the obtained results in terms of natural frequencies  $f_{i,exp}$ , damping  
 394 ratios  $\xi_{i,exp}$ , Coefficient of Variation CV and percentage differences  $\Delta$  before  
 395 and after rehabilitation. Mode shapes and MAC values are illustrated in

396 Figure 18. For the sake of brevity, only the modal features identified by the  
 397 SSI are shown.

Mode	Before		After		$\Delta_f$ [%]
	$f_{i,\text{exp}}$ [Hz]	$CV_f$ [%]	$f_{i,\text{exp}}$ [Hz]	$CV_f$ [%]	
1	2.15	1.85	2.56	0.21	+19.28
2	2.58	1.05	2.76	0.30	+6.70
3	4.98	0.69	7.15	0.27	+43.67
4	5.74	1.56	8.86	0.47	+54.37
5	6.76	1.13	9.21	0.21	+36.13
6	7.69	2.94	15.21	2.24	+97.87
7	8.98	1.21	16.91	1.40	+88.27
Avg	–	1.49	–	0.73	+49.47

Table 7: Dynamic response of Mogadouro tower before and after rehabilitation in terms of frequencies [44], [45].

Mode	Before		After		$\Delta_\xi$ [%]
	$\xi_{i,\text{exp}}$ [%]	$CV_\xi$ [%]	$\xi_{i,\text{exp}}$ [%]	$CV_\xi$ [%]	
1	2.68	219.51	1.25	0.13	-53.26
2	1.71	94.02	1.35	0.17	-21.00
3	2.05	65.33	1.20	0.14	-41.32
4	2.40	24.27	1.31	0.13	-45.72
5	2.14	31.74	1.16	0.12	-45.65
6	2.33	55.98	2.54	0.24	+9.11
7	2.30	46.39	1.49	0.23	-35.07
Avg	2.23	76.75	1.47	0.17	-40.34

Table 8: Dynamic response of Mogadouro tower before and after rehabilitation in terms of damping [44], [45].

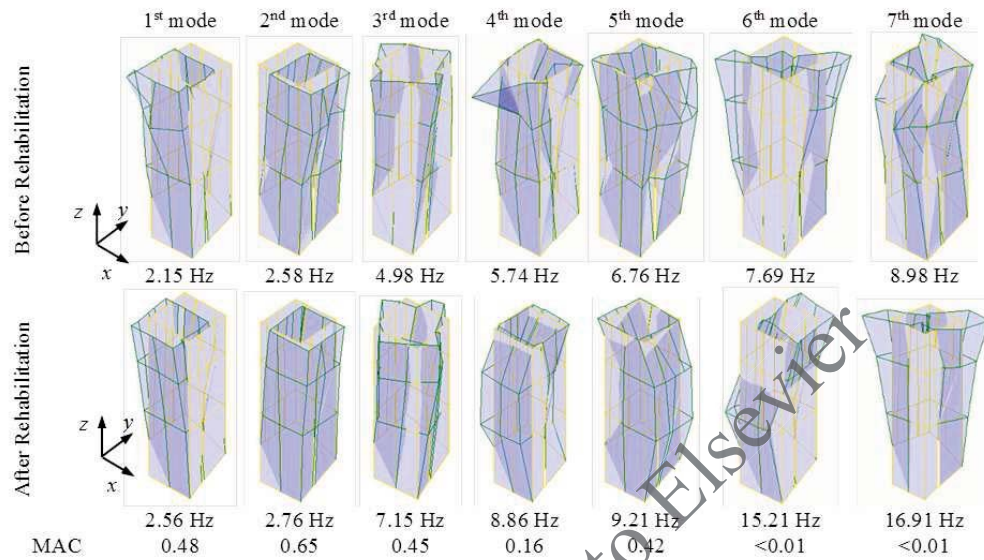


Figure 18: Experimental mode shapes and MAC values before and after rehabilitation works [44].

398 The comparison between the global parameters estimated before and after  
 399 the consolidation works revealed a significant increase of frequency values,  
 400 reading an average upshift of 50%, and a damping decrease of around 40%.  
 401 Such results consistently reflected the actual structural conditions of the  
 402 tower, i.e. a lower-stiffness system with ongoing non-linear phenomena effects  
 403 before rehabilitation and a higher-stiffness system with reduced non-linear  
 404 phenomena effects after rehabilitation. In what concerns the experimental  
 405 mode shapes, similar configurations were observed pre- and post-intervention  
 406 for the first five modes of vibration, identifying four dominant bending modes  
 407 in the two main planes of the tower (modes 1, 2, 4 and 5) and one torsional

408 mode (mode 3), whereas higher-frequency mode shapes (modes 6 and 7)  
409 switched order after the works. Although comparable in configuration, the  
410 presence of local damage mechanisms before the structural intervention did  
411 likely induce local protuberances in the experimental mode shapes of the  
412 damaged tower, especially in the upper part of the structure and in the areas  
413 close to the cracks. Hence the poor degree of correlation characterizing the  
414 mode shape vectors before and after ( $MAC < 0.65$ ). On the contrary, the  
415 structure featured a monolithic behaviour after the rehabilitation works.

#### 416 *4.3. Modal analysis with linear perturbation*

417 In this subsection the linear perturbation analysis is applied to the Mo-  
418 gadouro clock tower. The analysis is performed by using only NOSA-ITACA  
419 code for two reasons: (1) in DIANA, the Rankine plasticity model describing  
420 the tensile regime of the material is implemented only for plane stress, plane  
421 strain and axisymmetric elements, but not for brick elements, which are the  
422 ones employed in modeling the tower; (2) the MARC code turned out to be  
423 unable to reach the convergence for  $\sigma_t = 0$  Pa, a value that is crucial for a  
424 realistic modeling of eastern and western façades, where two passing cracks  
425 were present before rehabilitation.

426 In [44] and [45] a FE model updating (based on standard modal analysis) is  
427 performed to tune the Young's modulus of different parts of the structure, in  
428 order to minimize the differences between numerical and experimental modal  
429 parameters (frequencies and mode shapes) of the tower after rehabilitation;

430 subsequently, the Young's moduli obtained are reduced with the aim of fitting  
431 the experimental frequencies and mode shapes of the tower before rehabilita-  
432 tion. Here, a different approach is followed, based on model updating aimed  
433 at matching both fracture distribution and frequencies of the tower. With  
434 the purpose of reproducing numerically the actual crack pattern of the tower  
435 before rehabilitation and matching its experimental frequencies as well, the  
436 scheme described in Section 2 (nonlinear static analysis – linear perturba-  
437 tion – modal analysis) has been applied in an iterative way. In particular,  
438 once the solution to the equilibrium problem of the structure subjected to its  
439 own weight is calculated along with the corresponding fracture distribution,  
440 linear perturbation analysis and modal analysis are conducted to estimate  
441 frequencies and mode shapes of the tower in the presence of cracks. The  
442 materials Young's moduli and tensile strengths are tuned and their optimal  
443 values calculated in such a way as to match the crack distribution and mini-  
444 mize the discrepancy between experimental and numerical frequencies. The  
445 same procedure was then repeated to tune the tensile strength of the repaired  
446 walls, keeping the Young's moduli fixed and trying to match the experimen-  
447 tal natural frequencies and mode shapes of the tower after rehabilitation.

448 The FE mesh of the tower, shown in Figure 19, consists of 18024 isopara-  
449 metric 8–node brick elements, 352 thick shell elements, used to discretize  
450 the roof, and 23467 nodes; the model includes also two meters of foundation  
451 [44], [45] with the same thickness as the façades. The tower is assumed to  
452 be clamped at the base and constituted by the materials whose (optimal)

453 mechanical properties, calculated via model updating, are indicated in Table  
454 9. The foundation is modeled by a linear elastic material, which is indeed an  
455 acceptable assumption considering the high material compaction at the base  
456 of the tower and the soil confinement. Regarding pillars and roof, the use of  
457 a linear elastic material is suggested by the observation that these elements  
458 do not affect the overall structural behavior of the tower. Indeed, the low  
459 elastic modulus adopted for the roof does allow the tower cross section to  
460 freely deform within its own plane.

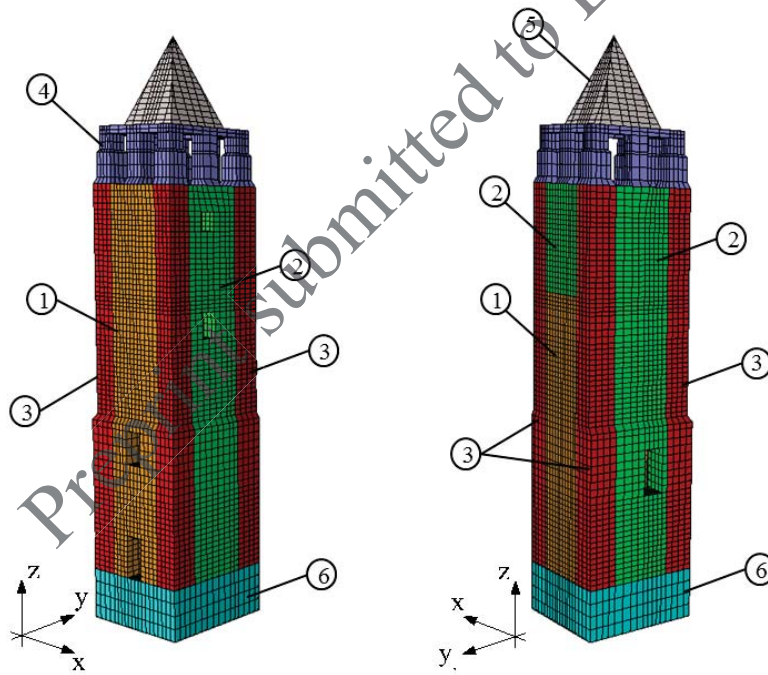


Figure 19: Mogadouro tower, mesh and distribution of material properties (before rehabilitation).

Mat. n°	Tower's portion	$\varrho[kg/m^3]$	$E[GPa]$	$\sigma_t[kPa]$
1 (orange)	façades South and North (bottom)	2200	2.500	15.0
2 (green)	façades East, West and North (top)	2200	2.500	0.0
3 (red)	corners	2400	3.500	15.0
4 (indigo)	pillars	2200	1.210	–
5 (grey)	roof	2000	0.195	–
6 (cyan)	foundation	2200	3.500	–

Table 9: Optimal values of the material mechanical properties before rehabilitation.

461 Numerical solution to the equilibrium problem for the optimal values of  
462 the Young's moduli and tensile strengths in Table 9 yields the results reported  
463 in Figures 20, 21 and 22 that show, for each façade, the actual (on the left)  
464 and numerical (on the right) crack patterns before rehabilitation. The South  
465 wall is not reported because it shows no cracks (neither in the numerical  
466 model nor in the reality). A very good agreement can be observed between  
467 real and numerical fracture strains.

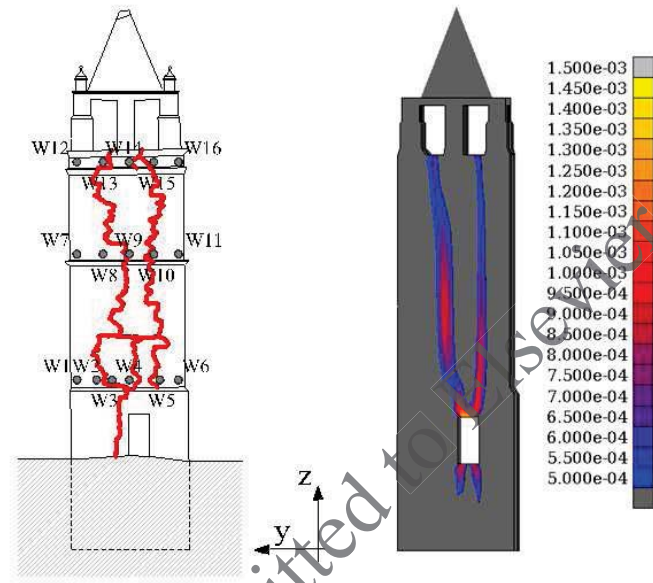


Figure 20: Mogadouro tower West façade, surveyed (on the left) and numerical (on the right) cracking pattern.

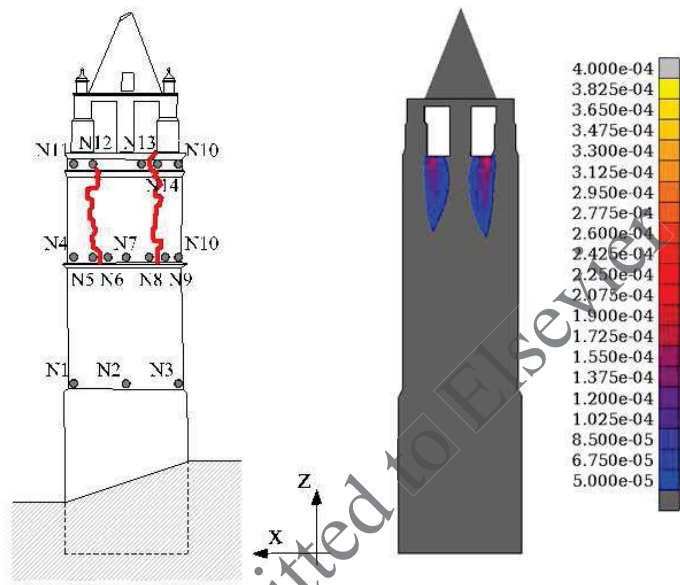


Figure 21: Mogadouro tower North façade, surveyed (on the left) and numerical (on the right) cracking pattern.

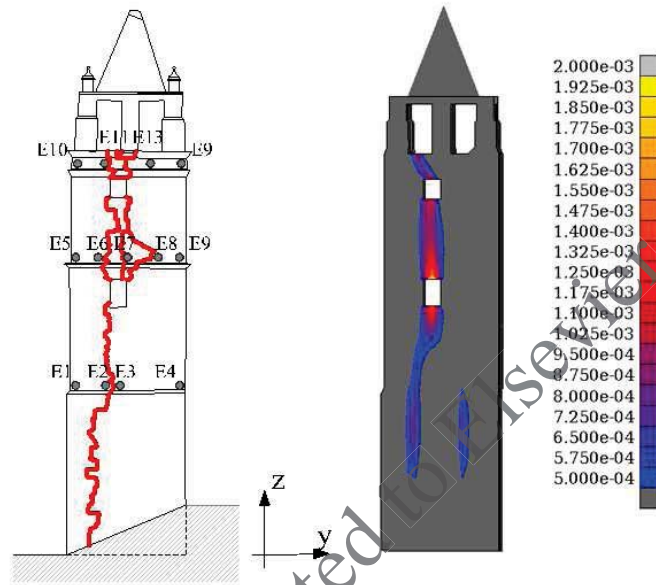


Figure 22: Mogadouro tower East façade, surveyed (on the left) and numerical (on the right) cracking pattern.

468 Table 10 summarizes the results of the modal analysis before rehabilita-  
 469 tion in terms of experimental ( $f_{i,exp}$ ) and numerical ( $f_{i,N}$ ) frequencies, relative  
 470 frequency error, and MAC values between experimental and numerical mode  
 471 shapes (evaluated considering just the nodes monitored during the experi-  
 472 mental campaigns [44], [45]). The four frequencies and the first two mode  
 473 shapes are very well approximated, while the correlation of the third and  
 474 fourth numerical mode shapes with their experimental counterparts is quite

475 low (particularly for the fourth mode). The poor match between the third  
 476 experimental and numerical mode shapes before rehabilitation is inherent to  
 477 the adopted modeling strategy and likely due to the fact that, as far as the  
 478 numerical solution is concerned, passing cracks in the East and West façades  
 479 do not allow the tower's section to undergo torsional deformations. On the  
 480 contrary, in the real case, such a deformation is made possible by interlocking  
 481 effect and friction between the units. It is also possible that other (non-visible  
 482 damage) can affect this mode.

Mode	$f_{i,\text{exp}}$ [Hz]	$f_{i,\text{N}}$ [Hz]	$\Delta_f$ [%]	MAC
1	2.15	2.15	0.00	0.94
2	2.58	2.60	-0.78	0.96
3	4.98	4.92	1.20	0.32
4	5.74	5.88	-2.44	0.01

Table 10: Comparison between experimental ( $f_{i,\text{exp}}$ ) and numerical frequencies ( $f_{i,\text{N}}$ ); relative frequency error  $\Delta_f = (f_{i,\text{exp}} - f_{i,\text{N}})/f_{i,\text{exp}}$  and MAC values before rehabilitation.

483 Figure 23 shows the first four experimental and numerical (calculated by  
 484 NOSA-ITACA) mode shapes of the Mogadouro tower before rehabilitation.

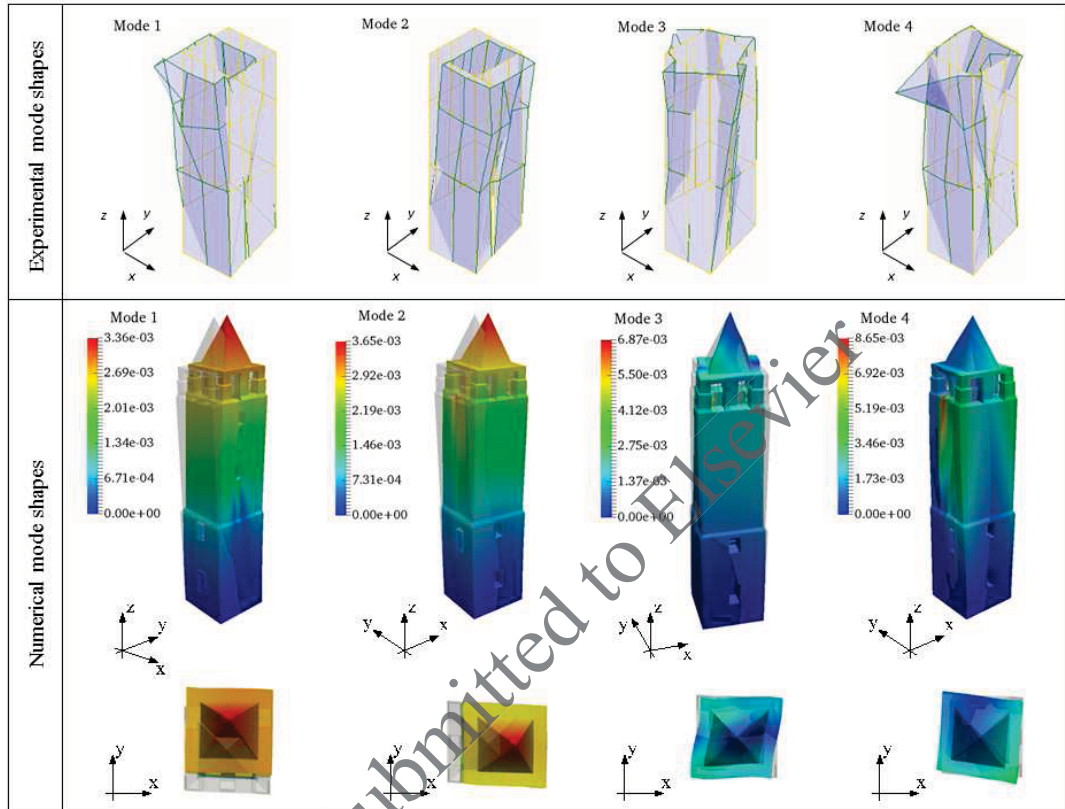


Figure 23: First four mode shapes of the Mogadouro tower before rehabilitation.

485 Subsequently, the same FE model is adopted to perform the analysis of  
 486 the tower after rehabilitation, considering a tensile strength  $\sigma_t = 10$  kPa  
 487 for the restored walls (material 2 in Figure 19), while the other mechanical  
 488 properties are kept fixed.

489 The results are summarized in table 11; Figure 24 shows the first four ex-  
 490 perimental and numerical mode shapes after rehabilitation. All frequencies  
 491 increase with respect to the unreinforced case, consistently with the exper-  
 492 imental results. In this case, a good approximation is achieved for all four

493 mode shapes, and a very great accuracy is obtained in the assessment of the  
 494 first two frequencies.

Mode	$f_{i,\text{exp}}$ [Hz]	$f_{i,\text{N}}$ [Hz]	$\Delta_f$ [%]	MAC
1	2.56	2.59	-1.17	0.98
2	2.76	2.75	0.36	0.98
3	7.15	8.39	-17.34	0.97
4	8.86	9.32	-5.19	0.74

Table 11: Comparison between experimental ( $f_{i,\text{exp}}$ ) and numerical frequencies ( $f_{i,\text{N}}$ ); relative frequency error  $\Delta_f = (f_{i,\text{exp}} - f_{i,\text{N}})/f_{i,\text{exp}}$  and MAC values after rehabilitation.

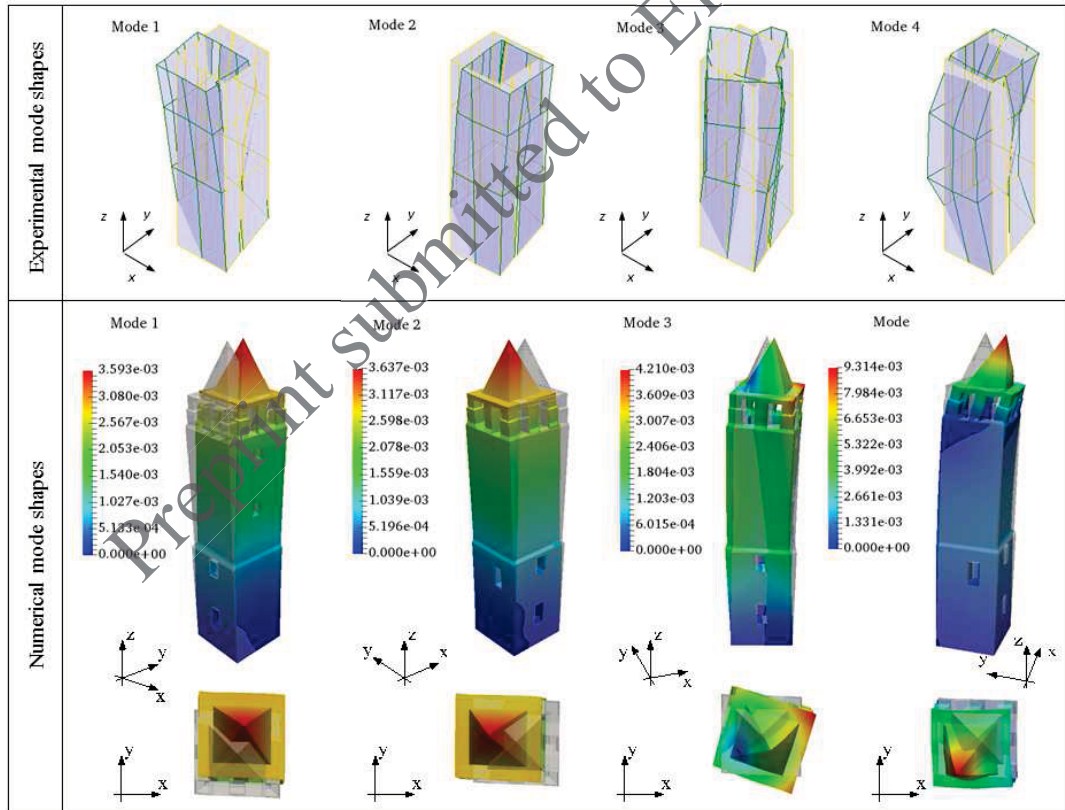


Figure 24: First four mode shapes of the Mogadouro tower after rehabilitation.

495 Table 12 recapitulates experimental and numerical results in terms of  
 496 natural frequencies, before and after rehabilitation of the tower, pointing out  
 497 that the linear perturbation analysis allows to catch the dynamic behavior  
 498 of the structure in damaged conditions with reasonable accuracy. The table  
 499 shows also that the numerical increase of the natural frequencies, due to  
 500 restoration of the tower and obtained in the numerical model through an  
 501 increase of tensile strength of the damaged walls, is in agreement with the  
 502 experimental results, apart from the third frequency, which is overestimated  
 503 by the code.

Mode	Before		After		$\Delta_f$ [%]	
	$f_{i,\text{exp}}$ [Hz]	$f_{i,\text{N}}$ [Hz]	$f_{i,\text{exp}}$ [Hz]	$f_{i,\text{N}}$ [Hz]	exp	num
1	2.15	2.15	<b>2.56</b>	2.59	+19.28	+20.46
2	2.58	2.60	<b>2.76</b>	2.75	+6.70	+5.77
3	4.98	4.92	7.15	8.39	+43.67	+70.52
4	5.74	5.88	8.86	9.32	+54.37	+58.50

Table 12: Summary of the experimental and numerical results before and after rehabilitation.

504 For the sake of comparison, the optimal values of the Young's modulus  $E_S$   
 505 calculated via a model updating based on standard modal analysis [44], [45]  
 506 are reported in table 13 together with the corresponding values  $E_{\text{NL}}$  obtained  
 507 by a model updating based on linear perturbation analysis. As expected, in  
 508 the standard modal analysis the lowest values of the Young's modulus are  
 509 obtained in the cracked façades.

	Before		After	
	$E_S$ [GPa]	$E_{LP}$ [GPa]	$E_S$ [GPa]	$E_{LP}$ [GPa]
South façade	0.687	2.500	1.974	2.500
North façade	2.210	2.500	2.210	2.500
West façade	0.302	2.500	1.075	2.500
East façade	0.276	2.500	0.804	2.500
Corners	3.870	3.500	3.875	3.500

Table 13: Comparison between the optimal values of the Young's modulus  $E_S$  (standard modal analysis) and  $E_{LP}$  (linear perturbation and modal analysis).

510 Tables 14 and 15 show the frequencies and MAC values calculated via  
511 standard modal analysis and linear perturbation analysis, before and after  
512 rehabilitation; for the sake of completeness the experimental frequencies are  
513 reported as well.

Mode	$f_{i,\text{exp}}$ [Hz]	Linear Perturbation			Standard		
		$f_i$ [Hz]	$\Delta_f$ [%]	MAC	$f_i$ [Hz]	$\Delta_f$ [%]	MAC
1	2.15	2.15	0.00	0.94	2.07	3.72	0.97
2	2.58	2.60	-0.78	0.96	2.40	6.98	0.97
3	4.98	4.92	1.20	0.32	5.14	-3.21	0.96
4	5.74	5.88	-2.44	0.01	5.88	-2.44	0.73

Table 14: Comparison between the frequencies calculated via standard modal analysis and linear perturbation before rehabilitation.

Mode	$f_{i,\text{exp}}$ [Hz]	Linear Perturbation			Standard		
		$f_i$ [Hz]	$\Delta_f$ [%]	MAC	$f_i$ [Hz]	$\Delta_f$ [%]	MAC
1	2.56	2.59	-1.17	0.98	2.54	0.78	0.99
2	2.76	2.75	0.36	0.98	2.68	2.90	0.99
3	7.15	8.39	-17.34	0.97	7.33	-2.52	1.00
4	8.86	9.32	-5.19	0.74	8.62	2.71	0.98

Table 15: Comparison between the frequencies calculated via standard modal analysis and linear perturbation after rehabilitation.

Preprint submitted to Elsevier

## 514 5. Conclusions

515 The present paper investigated the dependence of the dynamic properties  
516 of masonry structures on the nonlinear behavior of the constituent materials.  
517 As the mechanical response of masonry constructions is remarkably differ-  
518 ent in tension and in compression, and cracks may arise due permanent and  
519 accidental loads, standard modal analysis may result unrealistic. In this  
520 context, a linear perturbation approach must be used to adequately estimate  
521 the dynamic properties of masonry constructions in the presence of cracked  
522 regions. After a brief description of the constitutive equations and numer-  
523 ical procedures implemented in different FE codes (NOSA-ITACA, DIANA  
524 and MARC), the proposed approach, which couples linear perturbation and  
525 modal analysis, is described. The numerical procedure is then applied to  
526 a masonry arch with the aim of comparing and cross-validating the results  
527 obtained from the afore-mentioned FE codes in terms of natural frequencies  
528 and mode shapes for decreasing values of tensile strength. It is demonstrated  
529 that, despite the different constitutive equations the three codes rely on, the  
530 dependence of the dynamic properties of the masonry arch on the applied  
531 loads and induced crack distribution is consistent among the three of them,  
532 showing comparable frequency downshifts and MAC values over the different  
533 damage scenarios. Finally, with the purpose of validating the same approach  
534 on a real case-study structure, the procedure is applied to a historic masonry  
535 tower affected by a serious crack pattern. After solving the nonlinear equilib-  
536 rium problem of the structure subjected to its own weight and reproducing

537 the actual fracture distribution, a modal analysis about the equilibrium so-  
538 lution is carried out to estimate frequencies and mode shapes of the tower in  
539 the presence of cracks as well as after the rehabilitation works. A FE model  
540 updating is used to tune the optimal values for both Young's modulus and  
541 tensile strength in the different parts of the tower, according to the observed  
542 structural conditions before and after the intervention. The comparison be-  
543 tween numerical and experimental results showed that the combination of  
544 linear perturbation and modal analysis enables to estimate with reasonable  
545 accuracy the first two frequencies and mode shapes of the masonry tower in  
546 both damaged and reinforced conditions. The method proposed seems to be  
547 promising and further applications are necessary to confirm the reliability  
548 of the adopted approach for the solution of the dynamic problem in case of  
549 structures built with masonry materials.

550 **Acknowledgements.** This research has been partially supported by the  
551 Region of Tuscany (PAR-FAS 2007 – 2013) and MIUR, the Italian Ministry  
552 of Education, Universities and Research (FAR) within the Call FAR-FAS  
553 2014 (MOSCARDO Project: ICT technologies for structural monitoring of  
554 age-old constructions based on wireless sensor networks and drones, 2016 –  
555 2018) and by the Research Program Short-Term Mobility, funded by CNR,  
556 “Models, methods and tools for the structural analysis of ancient masonry  
557 constructions”, 2018. These supports are gratefully acknowledged.

- 558 [1] Alemdar Bayraktar, Ahmet Can Altunisik, Baris Sevim and Temel  
559 Türker, Seismic response of a historical masonry minaret using a fi-  
560 nite element model updated with operational modal testing. *Journal of*  
561 *Vibration and Control*, 17(1): 129-149, 2011.
- 562 [2] Altunisik A. C., Okur F. Y. , Fuat Genç A. , Günaydin, M., and Ada-  
563 nur, S., Automated model updating of historical masonry structures  
564 based on ambient vibration measurements. *Journal of Performance of*  
565 *Constructed Facilities*, 32(1): 04017126, 2018.
- 566 [3] Artemis Manual, Structural Vibration Solutions A/S, 2006.
- 567 [4] Azzara R.M., De Roeck G., Girardi M., Padovani C., Pellegrini D.,  
568 Reynders E., The influence of environmental parameters on the dy-  
569 namic behaviour of the San Frediano bell tower in Lucca. *Engineering*  
570 *Structures*, 156: 175-187, 2018.
- 571 [5] Azzara R.M., De Falco A., Girardi M., Pellegrini D., Ambient vibration  
572 recording on the Maddalena bridge in Borgo a Mozzano (Italy): Data  
573 analysis. *Annals of Geophysics*, 60(4): S0441, 2018.
- 574 [6] Bartoli G., Betti M., Vignoli A., A numerical study on seismic risk  
575 assessment of historic masonry towers: a case study in San Gimignano  
576 *A. Bull Earthquake Eng* 14: 1475, 2016.
- 577 [7] Bassoli E., Vincenzi L., D’Altri A.M, De Miranda S., Forghieri M.,  
578 Castellazzi G., Ambient vibration-based finite element model updat-

- 579 ing of an earthquake-damaged masonry tower. *Structural Control and*  
580 *Health Monitoring*, 25(5): e2150, 2018.
- 581 [8] Binante V, Girardi M, Padovani C, Pasquinelli G, Pellegrini D,  
582 Porcelli M., Robol L. *NOSA-ITACA 1.1 documentation* 2017.  
583 [www.nosaitaca.it/software/](http://www.nosaitaca.it/software/).
- 584 [9] Buyukozturk O., Nonlinear analysis of reinforced concrete structures.  
585 *Comput Struct*, 7: 149-156, 1977.
- 586 [10] Cabboi A., Gentile C. , Saisi A., From continuous vibration monitor-  
587 ing to FEM-based damage assessment: Application on a stone-masonry  
588 tower. *Construction and Building Materials* 156: 252-265, 2017.
- 589 [11] Camacho G.T., and Ortiz M., Computational modelling of impact dam-  
590 age in brittle materials. *Int J Solids Struct* 33: 2899-2938, 1996.
- 591 [12] Conde B., Ramos L.F. , Oliveira D.V., Riveiro B., Solla M., Structural  
592 assessment of masonry arch bridges by combination of non-destructive  
593 testing techniques and three-dimensional numerical modelling: Applica-  
594 tion to Vilanova bridge. *Engineering Structures* 148: 621-638, 2017.
- 595 [13] Debabrata Das, A new tangent stiffness-based formulation to study  
596 the free vibration behavior of a transversely loaded Timoshenko beam  
597 with geometric nonlinearity. *Journal of Vibration and Control*; **24(9)**:  
598 1716-1727, 2018.

- 599 [14] Del Piero G., Constitutive equation and compatibility of the external  
600 loads for linearly-elastic masonry-like materials. *Meccanica* 24: 150-62,  
601 1989.
- 602 [15] *DIANA-10.2 Finite Element Analysis, User's Manual-Release 10.2.*  
603 TNO, Netherlands, 2017.
- 604 [16] Dolatshahi K.M., Aref A.J., Yekrangnia M., Bidirectional behavior of  
605 unreinforced masonry walls. *Earthq. Eng. Struct. Dyn.* 43: 2377-2397,  
606 2014.
- 607 [17] Dolatshahi K.M., Aref A.J., Whittaker A.S., Interaction curves for  
608 in-plane and out-of-plane behaviors of unreinforced masonry walls. *J.*  
609 *Earthq. Eng.* 19: 60-84, 2015.
- 610 [18] Formisano A., Florio G., Landolfo R., Krstevska L., Tashkov Lj., Exper-  
611 imental and numerical investigation on a monumental masonry buiding  
612 damaged by the Abruzzo earthquake *8th International Conference on*  
613 *Structural Analysis of Historical Constructions SAHC 2012*, 2012.
- 614 [19] Feenstra P.H., Borst R., A plasticity model and algorithm for mode-I  
615 cracking in concrete. *Int. J. Numer. Methods Engrg.* 38: 2509-2529,  
616 1995.
- 617 [20] Feenstra P.H., Borst R., Crack band theory for fracture of concrete.  
618 *Materials and Structures*, RILEM, 93(16): 155-177, 1983.

- 619 [21] Gentile C., Guidobaldi M. and Saisi A., One-year dynamic monitor-  
620 ing of a historic tower: damage detection under changing environment.  
621 *Meccanica*, 51(11):2873–2889, 2016.
- 622 [22] Girardi M., Padovani C., Pellegrini D., The NOSA-ITACA code for  
623 the safety assessment of ancient constructions: A case study in Livorno.  
624 *Advances in Engineering Software* 89: 64-76, 2015.
- 625 [23] Girardi M., Padovani C., Pellegrini D., Modal analysis of masonry struc-  
626 tures. *Mathematics and Mechanics of Solids*, First Published February  
627 13, doi.org/10.1177/1081286517751837, 2018.
- 628 [24] Harak SS, Sharma SC, Harsha SP. Modal analysis of prestressed draft  
629 pad of freight wagons using finite element method. *J. Mod. Transport*  
630 2015; **23(1)**:43–49.
- 631 [25] Lagomarsino S., Penna A., Galasco A., Cattari S., TREMURI program:  
632 An equivalent frame model for the nonlinear seismic analysis of masonry  
633 buildings. *Engineering Structures* 56: 1787-1799, 2013.
- 634 [26] Lourenço P.B. , Oliveira D.V. , Milani G., Computational advances  
635 in masonry structures: from mesoscale modelling to engineering ap-  
636 plication. *Developments and Applications in Computational Structures*  
637 *Technology Saxe-Coburg Publications*, Chapter 1, pp. 1-23, 2010.
- 638 [27] Lourenço P.B. Computations on historic masonry structures. *Prog.*  
639 *Struct. Engng Mater.* 4: 301-319, 2002

- 640 [28] Lourenço P.B., Mendes N., Oliveira D.V., L.F. Ramos Possibilities and  
641 comparison of structural component models for the seismic assessment  
642 of modern unreinforced masonry buildings. *Computers and Structures*  
643 89, 2079-2091, 2011
- 644 [29] Lourenço P.B., Mendes N., Oliveira D.V., L.F. Ramos Analysis of ma-  
645 sonry structures without box behavior. *International Journal of Archi-  
646 tectural Heritage* 5:4-5, 369-382, 2011
- 647 [30] Lucchesi M., Padovani C., Pasquinelli G., Zani N. *Masonry construc-  
648 tions: mechanical models and numerical applications* 2008; Lecture  
649 Notes in Applied and Computational Mechanics. Springer-Verlag.
- 650 [31] Maia N.M.M. and Silva J.M.M. *Theoretical and experimental modal  
651 analysis*. Research Studies Press LTD., Baldock, Hertfordshire, England,  
652 1997.
- 653 [32] *Marc 2014 Volume A: theory and user information*. Marc & Mentat  
654 (2014) - Marc & Mentat Docs.
- 655 [33] Masciotta M.G., Ramos L.F., Lourenço P.B., The importance of struc-  
656 tural monitoring as a diagnosis and control tool in the restoration pro-  
657 cess of heritage structures: A case study in Portugal. *Journal of Cultral  
658 Heritage* 27: 36-47, 2017.
- 659 [34] Masciotta M.G., Ramos L.F., Lourenço P.B., Vasta M. Damage identifi-

- 660 cation and seismic vulnerability assessment of a historic masonry chim-  
661 ney. *Annals of Geophysics* 60(4),2017. doi: 10.4401/ag-7126 2017.
- 662 [35] Mistler M., Butenweg C., Meskouris K., Modelling methods of historic  
663 masonry buildings under seismic excitation. *J Seismol* 10: 497-510,  
664 2006.
- 665 [36] Noble D, Nogal M, O'Connor AJ, Pakrashi V. The effect of post-  
666 tensioning force magnitude and eccentricity on the natural bending fre-  
667 quency of cracked post-tensioned concrete beams. *Journal of Physics.*  
668 *Conference Series 628*, 2015. IOPscience.
- 669 [37] Oliveira D.V., Lourenço P.B., Implementation and validation of a con-  
670 stitutive model for the cyclic behaviour of interface elements. *Comput*  
671 *Struct* 82: 1451-61, 2004.
- 672 [38] Padovani C., Silhavy M., On the derivative of the stress-strain relation  
673 in a no-tension material. *Mathematics and Mechanics of Solids* 22: 1606-  
674 1618, 2017.
- 675 [39] Pantò B., Cannizzaro F., Calì I, Lourenço P.B., Numerical and experi-  
676 mental validation of a 3D macro-model for the in-plane and out-of-plane  
677 behavior of unreinforced masonry walls. *International Journal of Archi-*  
678 *tectural Heritage* 11.7: 946-964, 2017.
- 679 [40] Peeters B. and De Roeck G. One-year monitoring of the Z24-Bridge:

- 680 enviromental effects versus gamage events *Earthquake engineering and*  
681 *structural dynamics*, 30: 149–171, 2001.
- 682 [41] Pineda P. Collapse and upgrading mechanisms associated to the struc-  
683 tural materials of a deteriorated masonry tower. Nonlinear assessment  
684 under different damage and loading levels. *Engineering Failure Analysis*  
685 2016; **63**:72–93, Elsevier.
- 686 [42] Quagliarini E., Maracchini G., Clementi F. Uses and limits of the equiva-  
687 lent frame model on existing unreinforced masonry buildings for assess-  
688 ing their seismic risk: A review. *Journal of Building Engineering* 10:  
689 166-182, 2017.
- 690 [43] Ramos LF, De Roeck G, Lourenço PB, Campos–Costa A. Damage  
691 identification on arched masonry structures using ambient and random  
692 impact vibrations. *Engineering Structures* 2010; **32**: 146–162, Elsevier.
- 693 [44] L.F. Ramos , L. Marques , P.B. Lourenço , G.De Roeck , A. Campos-  
694 Costa and J.Roque. Monitoring historical masonry structures with op-  
695 erational modal analysis: two case studies. *Mech. Syst. Signal Process.*  
696 24: 1291-1305, 2010.
- 697 [45] L.F. Ramos Damage identification on masonry structures based on vi-  
698 bration signatures *Ph.D Thesis, University of Minho, Portugal*. Avail-  
699 able from [www.hms.civil.uminho.pt](http://www.hms.civil.uminho.pt), 2007.

- 700 [46] Ramos L.F., Núñez García A.C., Fernandes F.M. , Lourenço P.B. . Eval-  
701 uation of structural intervention in the Quartel das Esquadras, Almeida  
702 (Portugal). *Mech. Syst. Signal Process.* 24: 1291-1305, 2010.
- 703 [47] Rots J.G., Blaauwendraad J., Crack models for concrete, discrete or  
704 smeared? Fixed, multi-directional or rotating?. *HERON* 34.1, ISSN:  
705 0046-7316, 1989.
- 706 [48] Sacco E., A non linear homogenization procedure for periodic masonry.  
707 *Eur J Mech A/Solids* 28: 209-22, 2009.
- 708 [49] Sarhosis, Vasilis, Katalin Bagi, José V. Lemos, and Gabriele Milani,  
709 *Computational Modeling of masonry structures using the discrete el-*  
710 *ement method*, IGI Global, 2016: 1-505. Web. 16 May. 2018. doi:  
711 10.4018/978-1-5225-0231-9.
- 712 [50] Silva L.C., Lourenço P.B., Milani, G., Nonlinear discrete homogenized  
713 model for out-of-plane loaded masonry walls. *Journal of Structural En-*  
714 *gineering (United States)* 143.9: 1451-61, 2017.
- 715 [51] Taliercio A., Binda L., The Basilica of San Vitale in Ravenna: investi-  
716 gation on the current structural faults and their mid-term evolution. *J*  
717 *Cultural Heritage* 8: 99-118, 2007.
- 718 [52] Torres W., Almazán J.L., Sandoval C., Boroscsek R., Operational modal  
719 analysis and FE model updating of the Metropolitan Cathedral of San-  
720 tiago, Chile, *Engineering Structures* 143: 169-188, 2017.

721 [53] Treyssède F., Finite element modeling of temperature load effects on  
722 the vibration of local modes in multi-cable structures, *Journal of Sound*  
723 *and Vibration* 413: 191–204, 2018.

Preprint submitted to Elsevier